
Off-Policy RL Algorithms Can be Sample-Efficient for Continuous Control via Sample Multiple Reuse

Jiafei Lyu^{1*}, Le Wan² Zongqing Lu^{3†}, Xiu Li^{1†}

¹Tsinghua Shenzhen International Graduate School, Tsinghua University

²IEG, Tencent

³School of Computer Science, Peking University

lvjf20@mails.tsinghua.edu.cn, li.xiu@sz.tsinghua.edu.cn

Abstract

Sample efficiency is one of the most critical issues for online reinforcement learning (RL). Existing methods achieve higher sample efficiency by adopting model-based methods, Q-ensemble, or better exploration mechanisms. We, instead, propose to train an off-policy RL agent via updating on a fixed sampled batch multiple times, thus reusing these samples and better exploiting them within a single optimization loop. We name our method *sample multiple reuse* (SMR). We theoretically show the properties of Q-learning with SMR, e.g., convergence. Furthermore, we incorporate SMR with off-the-shelf off-policy RL algorithms and conduct experiments on a variety of continuous control benchmarks. Empirical results show that SMR significantly boosts the sample efficiency of the base methods across most of the evaluated tasks without any hyperparameter tuning or additional tricks.

1 Introduction

In recent years, the success of reinforcement learning (RL) has been witnessed in fields like games [67, 82, 96], neuroscience [14], fast matrix multiplication [25], and nuclear fusion control [16].

Online RL, different from batch RL [52], defines the task of learning an optimal policy via continual interactions with the environment. The agent can generally explore (discover unseen regions) and exploit (use what it already knows) [87] the data due to the accessibility to the environment. Prior work explores many exploration methods for both discrete [22, 10] and continuous control [61, 13] domains. With respect to the exploitation, off-policy deep RL algorithms are known to be more sample-efficient than on-policy methods, as they usually store past experiences and reuse them during training. Unfortunately, most of the off-policy deep RL algorithms, especially on continuous control domains, still need a vast number of interactions to learn meaningful policies. Such a phenomenon undoubtedly barriers the wide application of RL algorithms in real-world problems, e.g., robotics.

In this paper, we set our focus on continuous control domains. There are many efforts in enhancing the exploration capability of the off-policy RL algorithms by adding extra bonus reward [90, 28, 42, 1], leveraging maximum entropy framework [109, 30, 31], etc. Another line of research focuses on better exploiting the data. They achieve this by alleviating the overestimation bias in value estimate [29, 56, 50, 64], using high update-to-data (UTD) ratio [11, 41], adopting model-based methods [44, 51, 71, 102], etc. Nevertheless, these advances often involve complex components like ensemble. We wonder: *is it possible to design a simple method that can universally better exploit data and improve sample efficiency?*

To this end, we propose *sample multiple reuse* (SMR), where we update the actor and the critic network multiple times on the fixed sampled batch data, as shown in Figure 1. By doing so, the

*Work done while working as an intern at Tencent IEG. † Corresponding Authors.

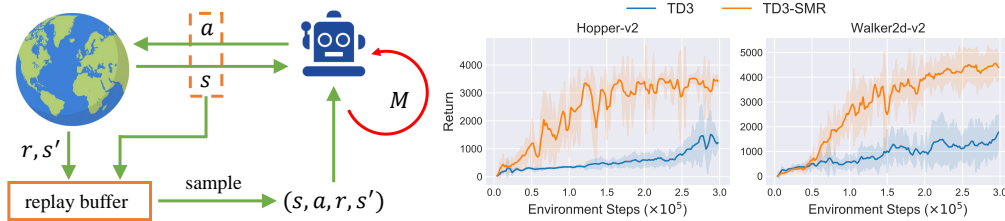


Figure 1: **Left:** the key idea behind Sample Multiple Reuse (SMR) lies in the **red arrow** where we update the agent on the fixed samples for M times. **Right:** SMR significantly boosts the sample efficiency of TD3 [29].

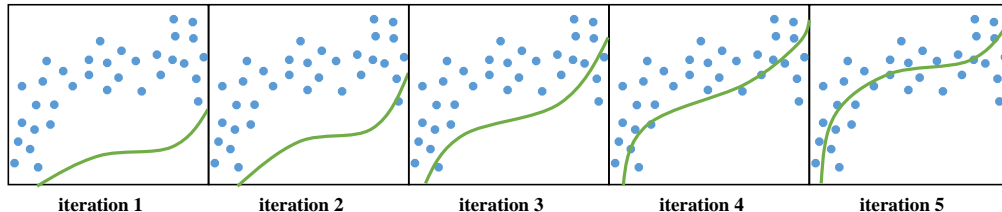


Figure 2: The key idea illustration of sample multiple reuse. The **blue** dots represent the samples in a batch. With only one iteration, it is hard for the approximator (e.g., neural network) to well-fit the data. Whereas, with more updates on the identical batch, the approximator can better fit the samples.

networks can better fit and exploit the batch data (as depicted in Figure 2). We deem that every collected sample from online interaction is valuable and is worth being utilized more times during training. SMR is general and can be combined with *any* off-the-shelf off-policy continuous control RL algorithms by modifying only a few lines of code.

To illustrate the rationality and benefits of SMR, we combine it with Q-learning and propose Q-SMR algorithm. We theoretically analyze the convergence property of Q-SMR in the tabular case. We empirically show that Q-SMR exhibits stronger sample efficiency than vanilla Q-learning. We then combine SMR with five typical continuous control RL algorithms and run experiments on four tasks from OpenAI Gym [8]. We combine SMR with SAC [30] and extensively evaluate SAC-SMR on two additional continuous control benchmarks, yielding a total of 30 tasks. Across most of the evaluated tasks, we observe improvement in sample efficiency over the base algorithms, often by a large margin (as shown in Figure 1). The empirical results reveal that SMR is very general and can improve the sample efficiency of different algorithms in a variety of tasks.

To ensure that our proposed method is reproducible [43, 38], we include the anonymous code in <https://anonymous.4open.science/r/SMR-F3F2>, and evaluate the experimental results across fair evaluation metrics.

2 Preliminaries

Reinforcement learning (RL) aims at dealing with sequential decision-making tasks. It can be formulated as a Markov decision process (MDP) defined by a tuple $\langle \mathcal{S}, \mathcal{A}, r, p, \gamma \rangle$. \mathcal{S} is the state space, \mathcal{A} is the action space, $r : \mathcal{S} \times \mathcal{A} \mapsto \mathbb{R}$ is the scalar reward signal, $p(\cdot | s, a)$ is the dynamics transition probability, and $\gamma \in [0, 1)$ is the discount factor. In online RL, the agent can continually interact with the environment by following a policy $\pi : \mathcal{S} \mapsto \mathcal{A}$. The goal of the agent is to maximize the expected discounted long-term rewards, i.e.,

$$\max J(\phi) = \mathbb{E} \left[\sum_{t=0}^{\infty} \gamma^t r(s_t, a_t) \middle| s_0, a_0; \pi \right]. \quad (1)$$

A policy is said to be *stationary* if it is time-invariant. The state-action value function (also Q -function) $Q^\pi : \mathcal{S} \times \mathcal{A} \mapsto \mathbb{R}$ given a policy π is defined by

$$Q^\pi(s, a) = \mathbb{E}_\pi \left[\sum_{t=0}^{\infty} \gamma^t r(s_t, a_t) \middle| s_0 = s, a_0 = a \right]. \quad (2)$$

The optimal Q -function Q^* is the unique fixed point of the Bellman operator $\mathcal{T}Q$, which is given by:

$$\mathcal{T}Q(s, a) := r(s, a) + \gamma \mathbb{E}_{s' \sim p(\cdot|s, a)} [\max_{a' \in \mathcal{A}} Q(s', a')]. \quad (3)$$

A typical off-policy RL algorithm is Q-learning [99]. It aims at learning the optimal Q -function and updates its entry via the following rule:

$$Q_{t+1}(s, a) = (1 - \alpha_t)Q_t(s, a) + \alpha_t(r_t + \gamma \max_{a' \in \mathcal{A}} Q_t(s', a')), \quad (4)$$

where α_t is the learning rate at timestep t .

3 Why Not Reuse Your Data More?

In online deep RL, it is a common practice that we sample a mini-batch in a bootstrapping way from the replay buffer, where the past experience is stored, for training the RL agent. However, existing off-policy RL methods only evaluate *once* upon the sampled transitions, which is a waste since they fail to better exploit the collected valuable samples.

We remedy existing off-policy RL algorithms by reusing the sampled batch data more times. Our key intuition and motivation lie in the fact that it is hard for the neural network to well-fit and well-evaluate the sampled batch with just one glance (check Figure 2). With more updates on the sampled batch, the network can better adapt to the sample distribution, in conjunction with a more reliable evaluation upon them. We name our method *sample multiple reuse* (SMR), which can be combined with *any* off-policy RL algorithms. We first combine our method with vanilla Q-learning [99], yielding the Q-SMR algorithm as depicted in Algorithm 1. We further define the number of iterations M as the SMR ratio, which measures the fixed batch reusing frequency of the agent. Empirically, Figure 3 illustrates the superior sample efficiency of our proposed Q-SMR algorithm against vanilla Q-learning in the tabular case, where a fixed $M = 10$ is utilized for the Q-SMR. In both the classical cliff-walking environment and a maze environment, Q-SMR is able to learn faster and converge faster.

Algorithm 1 Q-SMR

- 1: Set learning rate sequence $\{\alpha_t\}$, number of iterations T .
 - 2: Initialize $Q(s, a)$ table with 0.
 - 3: **for** $t = 1$ to T **do**
 - 4: Choose action a derived from Q , e.g., ϵ -greedy, and observe reward r and next state s' .
 - 5: **for** $m = 1$ to M **do**
 - 6: Update Q_t according to Equation 4.
 - 7: **end for**
 - 8: **end for**
-

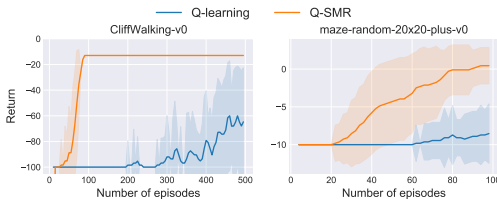


Figure 3: Comparison of Q-SMR and Q-learning on CliffWalking-v0 and maze-random-20x20-plus-v0 tasks from Gym [8]. The results are averaged over 20 independent runs, and the shaded region is the standard deviation.

Moreover, our method can also be incorporated with any off-policy (deep) RL algorithms, and the experimental results in Figure 3 shed light on doing so. We detail the (abstracted) off-policy actor-

Algorithm 2 Off-policy actor-critic with SMR

- 1: Initialize critic network parameter θ , actor network parameter ϕ with random parameters.
 - 2: Initialize target critic network parameter $\theta' \leftarrow \theta$.
 - 3: Initialize empty replay buffer $\mathcal{B} = \{\}$.
 - 4: (Optional) Initialize target actor network parameter $\phi' \leftarrow \phi$.
 - 5: **for** $t = 1$ to T **do**
 - 6: Choose action a and observe reward r , next state s' .
 - 7: Store the transition in the replay buffer, i.e., $\mathcal{B} \leftarrow \mathcal{B} \cup \{(s, a, r, s')\}$.
 - 8: Sample N transitions $\{(s_j, a_j, r_j, s'_j)\}_{j=1}^N$ from \mathcal{B} .
 - 9: **for** $m = 1$ to M **do**
 - 10: Update critic by minimizing Bellman error.
 - 11: Update actor with policy gradient.
 - 12: Update target network.
 - 13: **end for**
 - 14: **end for**
-

critic with SMR in Algorithm 2. Compared to typical actor-critic methods, our revised algorithm only enforces the agent to train on identical batch data multiple times. This requires a minimal change to the base algorithm, which can be completed by modifying a few lines of code. We defer the detailed pseudo-code of various off-policy algorithms with SMR in Appendix D.

4 Theoretical Analysis

In this section, we aim at showing the theoretical properties of the Q-SMR algorithm in the tabular case. The theoretical guarantee of Q-SMR can pave the way for applying SMR in complex continuous control tasks. All missing proofs can be found in Appendix B.

We consider asynchronous Q-learning [24, 59] which follows the update rule:

$$\begin{aligned} Q_{t+1}(s_t, a_t) &= (1 - \alpha_t)Q_t(s_t, a_t) + \alpha_t \mathcal{T}_{t+1}Q_t(s_t, a_t), \\ Q_{t+1}(s, a) &= Q_t(s, a) \quad \forall (s, a) \neq (s_t, a_t), \end{aligned} \quad (5)$$

where $\mathcal{T}_{t+1}Q_t(s_t, a_t) = r_t + \gamma \max_{a' \in \mathcal{A}} Q_t(s_{t+1}, a')$. We have access to a sample trajectory $\{s_t, a_t, r_t\}_{t=0}^{\infty}$ from a behavior policy π_b , and we only update one (s, a) -entry each step here.

Given the SMR ratio M , we define $Q_t^{(i)}(s, a), i \in [1, M]$ as the intermediate Q -function at timestep t and iteration i . The resulting Q -function after SMR iteration is $Q_t(s, a)$ where we omit superscript (M) for $Q_t(s, a)$. We define $Q_{t+1}^{(0)}(s, a) = Q_t^{(M)}(s, a)$. We first give the update rule for Q-SMR that is equivalent to the loop (line 4-6 in Algorithm 1) in Theorem 1.

Theorem 1. *The update rule of Q-SMR is equivalent to:*

$$\begin{aligned} Q_{t+1}(s_t, a_t) &= (1 - \alpha_t)^M Q_t(s_t, a_t) + \sum_{i=0}^{M-1} \alpha_t (1 - \alpha_t)^i \mathcal{T}_{t+1} Q_{t+1}^{(M-1-i)}(s_t, a_t), \\ Q_{t+1}(s, a) &= Q_t(s, a) \quad \forall (s, a) \neq (s_t, a_t), \end{aligned} \quad (6)$$

where $\mathcal{T}_{t+1}Q_{t+1}(s_t, a_t) = r_t + \gamma \max_{a' \in \mathcal{A}} Q_{t+1}(s_{t+1}, a')$ denotes the empirical Bellman operator w.r.t. timestep $t + 1$.

Remark: The update rule of Q-SMR relies on the intermediate value during the SMR iteration. The influence of the current Q-value in Q-SMR is reduced (as $(1 - \alpha_t)^M \leq (1 - \alpha_t)$), and hence the value estimate can change faster by querying the maximal value. This we believe can partly explain the superior sample efficiency of Q-SMR against vanilla Q-learning depicted in Figure 3.

Assumption 1. *Assume that $\forall t$, the reward signal is bounded, $|r_t| \leq r_{\max}$.*

We note that this is a widely used assumption, which can also be easily satisfied in practice as many reward functions are hand-crafted. We then show in Theorem 2 that Q-SMR outputs a bounded value estimate throughout its iteration.

Theorem 2 (Stability). *Let Assumption 1 hold and assume the initial Q-function is set to be 0, then for any iteration t , the value estimate induced by Q-SMR, \hat{Q}_t , is bounded, i.e., $|\hat{Q}_t| \leq \frac{r_{\max}}{1 - \gamma}, \forall t$.*

We further show that the Q-SMR algorithm is guaranteed to converge to the optimal Q-value, which reveals the rationality of utilizing the Q-SMR algorithm in practice and paves the way for extending the Q-SMR algorithm into deep RL scenarios.

Theorem 3 (Convergence). *Under some mild assumptions that are similar to [29, 66], the Q-SMR algorithm converges to the optimal Q-function.*

Interestingly, we can establish a connection between modified learning rate and SMR update rule by assuming that the underlying MDP is *nonreturnable*, i.e., $s_{t+1} \neq s_t$. Then, the rule can be simplified.

Corollary 1. *If the MDP is nonreturnable, the update rule of Q-SMR gives:*

$$\begin{aligned} Q_{t+1}(s_t, a_t) &= (1 - \alpha_t)^M Q_t(s_t, a_t) + [1 - (1 - \alpha_t)^M] \mathcal{T}_{t+1}Q_t(s_t, a_t), \\ Q_{t+1}(s, a) &= Q_t(s, a) \quad \forall (s, a) \neq (s_t, a_t). \end{aligned} \quad (7)$$

Remark: Compared to vanilla Q-learning, this rule actually *modifies* the learning rate from α_t to $1 - (1 - \alpha_t)^M$. Since $\alpha_t \in [0, 1]$, it is easy to see $1 - (1 - \alpha_t)^M \in [0, 1], \forall t$.

Furthermore, we can derive the finite time error bound of the Q-SMR algorithm based on the above corollary, which improves over the prior results [88, 24, 76]. Please refer to Appendix A for more details and discussions.

5 Experiments

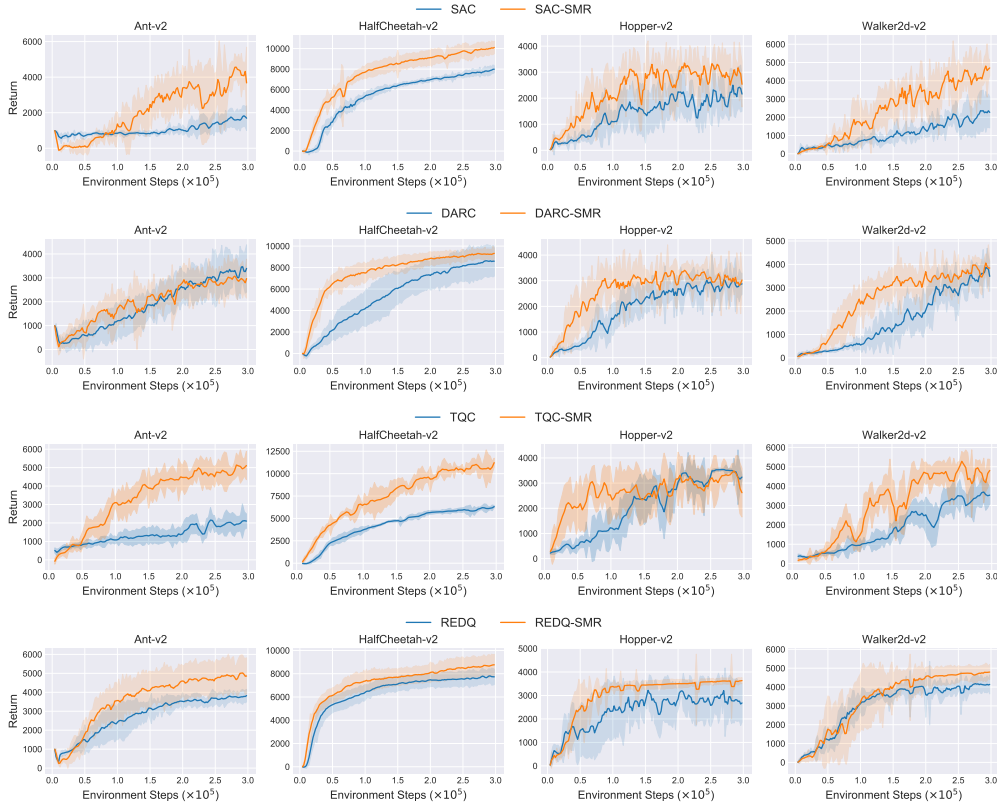


Figure 4: Experimental results of four typical continuous control algorithms with and w/o SMR on four OpenAI Gym [8] environments. The results are averaged over 6 independent runs. The shaded region denotes the standard deviation.

In this section, we investigate the benefits of SMR upon off-the-shelf off-policy continuous control RL algorithms. We aim at answering the following questions: (1) is the SMR general enough to benefit wide off-policy RL algorithms? (2) how much performance gain can off-policy RL algorithms acquire by using SMR?

In order to show the strong data exploitation ability and the generality of SMR, we combine SMR with TD3 [29], SAC [31], DARC [64], TQC [50], and REDQ [11]. We choose these methods as they typically represent different categories of continuous control algorithms, i.e., TD3 leverages clipped double Q-learning, SAC is based on the maximum entropy RL, DARC enhances the agent’s exploration capability by using double actors, TQC addresses overestimation by incorporating distributional RL into the continuous setting, and REDQ is the state-of-the-art model-free RL method which trains critic ensemble and uses a high update-to-data (UTD) ratio.

Besides the loop of reusing samples (line 5-9 in Algorithm 2), we do not make any additional modifications (e.g., parameter tuning) to the base algorithm. We run experiments on four continuous control tasks from OpenAI Gym [8] simulated by MuJoCo [92]. All methods are run for 300K online interactions where we adopt the SMR ratio $M = 10$ by default except REDQ where we set $M = 5$

(as REDQ already uses a large UTD ratio). We note that 300K is a typical interaction step adopted widely in prior work [11, 44, 36] for examining sample efficiency.

Each algorithm is repeated with 6 random seeds and evaluated over 10 trials every 1000 timesteps. We find that SMR significantly improves the sample efficiency of the base algorithms on almost every task, often outperforming them by a large margin (see Figure 4). SAC-SMR achieves 4x and TQC-SMR has 3x sample efficiency than the base algorithm as shown in Table 1. Notably, SAC-SMR takes only 93K online interactions to reach 3000 in Hopper-v2, and TQC-SMR takes merely 34K online interactions. The results even match the performance of MBPO [44] (around 73K). We show in Appendix C that other off-policy RL algorithms like DDPG, DrQ-v2 [103] can benefit from SMR as well. These altogether reveal that **the advantage of SMR is algorithm-agnostic**.

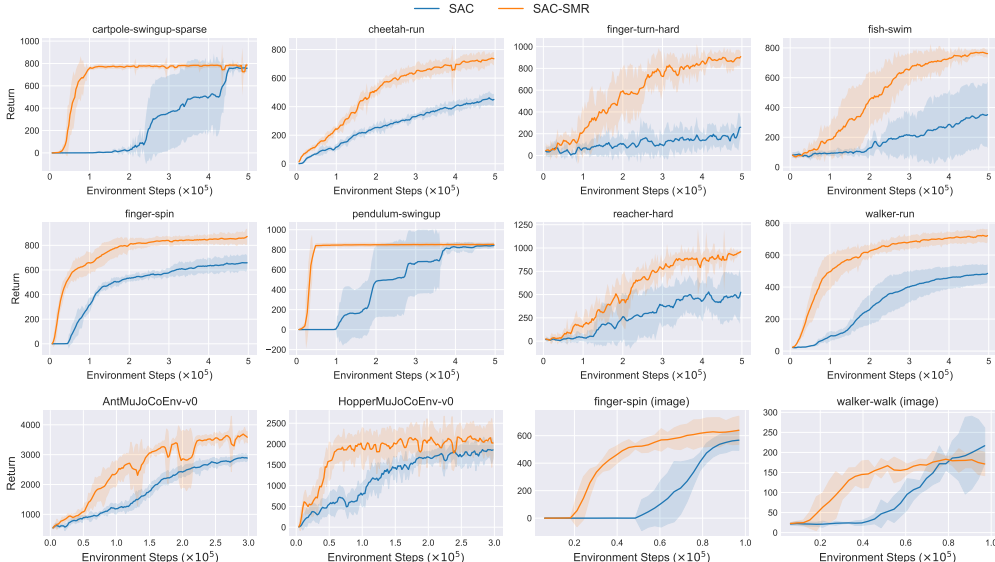


Figure 5: Experimental results of SAC-SMR against vanilla SAC on 8 state-based, 2 image-based DMC suite [91] tasks and 2 PyBullet-Gym [23] tasks. The results are averaged over 6 seeds. The shaded region captures the standard deviation.

Table 1: Sample efficiency comparison. We choose SAC, TQC and DARC as examples. The numbers indicate the number of online interactions when the specified performance level is reached.

Score	SAC	SAC-SMR	TQC	TQC-SMR	DARC	DARC-SMR
Hopper@3000	373K	93K	160K	34K	205K	67K
Ant@4000	982K	211K	469K	135K	324K	305K
HalfCheetah@10000	860K	282K	576K	185K	407K	324K
Walker2d@4000	656K	164K	281K	133K	292K	264K

We further combine SMR with SAC and run SAC-SMR extensively on two additional continuous control benchmarks, DMC suite [91] and PyBullet-Gym [23]. We conduct experiments on 20 DMC suite tasks, 4 PyBullet-Gym tasks, and 6 image-based tasks from DMC suite, yielding a total of **30** tasks. For state-based tasks, we use $M = 10$ and run for 500K interactions. For image-based tasks, as it is very time-consuming with $M = 10$, we use $M = 5$, which we find is sufficient to show the advantage of SMR. Both SAC and SAC-SMR are evaluated over 10 trials every 1000 timesteps. It can be seen in Figure 5 that SMR significantly boosts the sample efficiency of SAC on the evaluated tasks. This can also be validated from Table 2 where SAC-SMR achieves 2.5x the performance of SAC at 250K and 2.0x the performance of SAC at 500K when averaging the numbers.

Due to the space limit, we defer some results to Appendix C and only report a small proportion of tasks here. These experimental results show that **the advantage of SMR is task-agnostic**. In summary, we believe the above evidence is enough to verify the generality and effectiveness of SMR.

Parameter Study. The most critical hyperparameter in our method is the SMR ratio. It controls the frequency we reuse a fixed batch. Intuitively, we ought not to use too large M to prevent potential

Table 2: Performance comparison of SAC, SAC-UTD (UTD ratio $G=10$) and SAC-SMR. We choose cheetah-run and fish-swim as examples. The numbers indicate the performance achieved when the specific number of data is collected. \pm captures the standard deviation.

Amount of data	SAC	SAC-UTD	SAC-SMR
cheetah-run@250K	284.6 \pm 20.5	434.1 \pm 72.6	600.1 \pm 49.2
fish-swim@250K	178.5 \pm 113.9	382.5 \pm 70.7	544.3 \pm 184.4
cheetah-run@500K	452.1 \pm 47.7	633.9 \pm 99.1	725.4 \pm 48.7
fish-swim@500K	324.8 \pm 213.9	712.0 \pm 41.9	756.3 \pm 38.7

overfitting in neural networks. For state-based tasks, we find that setting $M = 10$ can incur very satisfying performance. In order to see the influence of the SMR ratio M , we conduct experiments on Ant-v2 and HalfCheetah-v2 from OpenAI Gym [8]. We sweep M across $\{1, 2, 5, 10, 20\}$ and demonstrate in Figure 6 that SMR can improve the sample efficiency of the base algorithm even with a small $M = 2$, and the sample efficiency generally increases with larger M . We do not bother tuning M and keep it fixed across our experiments.

Computation Budget. SMR consumes more computation budget than its base algorithm due to multiple updates on the fixed batch. Intuitively, our method will require more training time with a larger SMR ratio M . Typically, SMR ($M = 10$) will take about 3-5 times of more training time, e.g., SAC-SMR takes around 6 hours for 300K interactions on Walker2d-v2, while SAC takes around 1.5 hours. Such cost is tolerable for *state-based* tasks considering the superior sample efficiency improvement with SMR.

Clarification on the Asymptotic Performance. As we focus on improving the sample efficiency, the asymptotic performance of SMR upon different base methods lies out of the scope of this work. Nevertheless, readers of interest can find that the asymptotic performance of SMR is quite good (please refer to Appendix C.3 where we run SMR upon different algorithms for longer interactions).

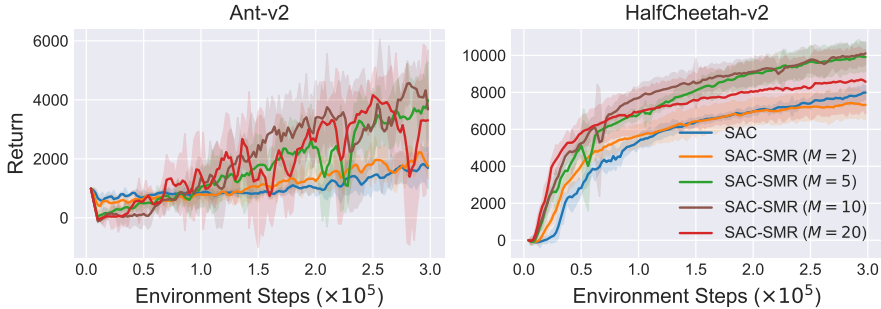


Figure 6: The performance of SAC-SMR under different SMR ratios on two selected environments. The results are averaged over 6 runs and the shaded area captures the standard deviation.

6 Discussions

6.1 Is SMR equivalent to enlarging learning rate?

One may think that SMR is equivalent to amplifying learning rate M times at first sight, i.e., $\alpha_t \rightarrow M\alpha_t$. Whereas, we argue that they are *quite different*. In the tabular case, we show in Theorem 1 the update rule for Q-SMR, which is obviously not the rule that enlarges the original learning rate sequence M times. In deep RL, suppose the (single) critic and actor are parameterized by θ and ϕ , respectively. The objective function of the critic gives:

$$\mathcal{L}_\theta = \mathbb{E}_{s,a,s' \sim \rho} [(Q_\theta(s,a) - r - \gamma Q_{\theta'}(s',a'))^2], \quad (8)$$

where $a' \sim \pi_\phi$, ρ is the sample distribution in the replay buffer, θ' is the parameter of the target network. Deep neural networks are typically trained with stochastic gradient descent (SGD) [54, 63, 7]. The critic is optimized using the gradient information $\nabla \mathcal{L}_{\theta_t}$ obtained on the t -th batch, i.e., $\theta_{t+1} = \theta_t - \alpha_t \nabla \mathcal{L}_{\theta_t}$. We then show that, in deep RL, SMR is also not equivalent to enlarging learning rate.

Theorem 4. Denote $\theta_t^{(i)}$ as the intermediate parameter in the SMR loop at timestep t and iteration i , then in deep RL, the parameter update using SMR satisfies:

$$\theta_{t+1} = \theta_t - \alpha_t \sum_{i=0}^{M-1} \nabla \mathcal{L}_{\theta_{t+1}^{(i)}} \neq \theta_t - M\alpha_t \nabla \mathcal{L}_{\theta_t}. \quad (9)$$

The inequality in the above theorem is due to the fact that $\theta_{t+1}^{(i+1)} \neq \theta_{t+1}^{(i)}$. A natural question is then raised: how does SMR compete against magnifying the learning rate?

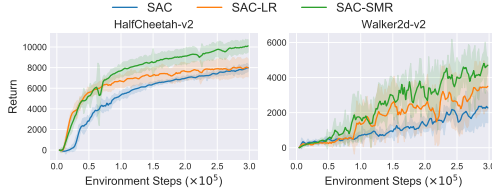


Figure 7: Comparison of SAC-SMR ($M = 10$) against SAC-LR (i.e., amplify the learning rate 10 times). Each algorithm is repeated with 6 seeds and evaluated over 10 trials every 1000 timesteps. We report the mean performance and the standard deviation.

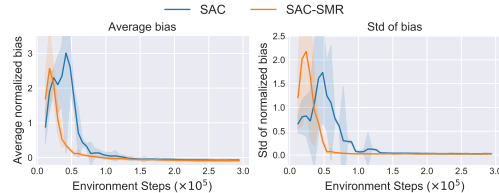


Figure 8: Normalized bias comparison of SAC and SAC-SMR on HalfCheetah-v2. SAC-SMR exhibits overfitting at first (with both larger average bias and std of bias) while can incur smaller estimation bias very quickly.

We answer this by conducting experiments on two selected environments from OpenAI Gym [8]. Empirical results in Figure 7 show that enlarging the learning rate does aid performance gain, yet it still underperforms SMR in sample efficiency. It is trivial to find the best learning rate. SMR, instead, can benefit the base algorithm with the default parameter (see more evidence in Appendix C).

6.2 Concerns on overfitting

One may wonder whether the phenomenon of overfitting [18, 85] will occur in SMR since we optimize the networks on fixed samples for multiple times. The networks may overfit the collected samples at first, but they can get rid of this dilemma and end up with better data exploitation later on with *reasonable* M . We verify this by measuring the accuracy of $Q^\pi(s, a)$ over the state-action distribution of the current policy π against its true value $Q(s, a)$ (i.e., discounted Monte Carlo return). Since the Monte Carlo return can change drastically during training, we adopt normalized estimation bias $\frac{Q^\pi(s, a) - Q(s, a)}{|\mathbb{E}_{s, a \sim \pi}[Q(s, a)]|}$ for more meaningful comparison. We conduct experiments on HalfCheetah-v2. We run each algorithm with 6 seeds for 300K online interactions and evaluate them over 10 trials every 1000 timesteps. We adopt the same way of calculating the normalized estimation bias as REDQ [11]. As illustrated in Figure 8, SMR incurs slight overfitting at the beginning of training, while it can quickly escape from it and result in a smaller estimation bias afterwards.

This may be because the networks can well-fit new transitions from continual online interactions with multiple updates. Since SMR uses much fewer gradient steps per interaction with the environment compared with REDQ (with UTD $G = 20$), we believe the concerns on overfitting can be mitigated to some extent. As a piece of evidence, we do not find any performance degradation with $M = 10$ across a wide range of algorithms and tasks. The key for not overfitting is the appropriate choice of SMR ratio M . No wonder that it will be hard for the agent to get rid of overfitting with too large M (e.g., $M = 10^5$, also referred to as *heavy priming* phenomenon in [70]). For those who still worry about overfitting, we can remedy this by: (1) using a small M , e.g., $M = 5$; (2) resetting the agent periodically [70] such that it forgets past learned policy; (3) leveraging a larger batch size; etc. Note that one does not have to stick to adopting a high SMR ratio throughout the training process, and can use SMR as a *starting point*, or a warm-up phase, e.g., one can use $M = 10$ for 300K interactions and then resume vanilla training process (i.e., $M = 1$), which can also relieve potential overfitting.

6.3 Comparison with UTD (update-to-data)

SMR focuses on boosting the sample efficiency of model-free algorithms by better exploiting collected samples. This is similar in spirit to model-based methods (e.g., MBPO [44]) and REDQ [11] as they

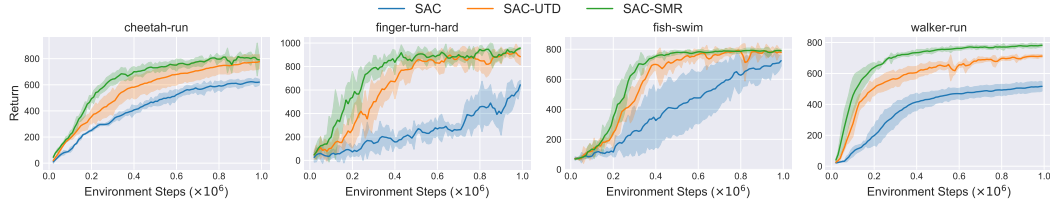


Figure 9: Comparison of SAC-SMR ($M = 10$) against SAC-UTD ($G = 10$) under identical update frequency. The results are averaged over 6 runs, and the standard deviation is also reported.

usually employ a large update-to-data (UTD) ratio, i.e., update the critic multiple times by sampling with bootstrapping (the sampled batch is different each time). However, SMR updates both actor and critic on the *fixed* sampled batch multiple times to better fit the data (as Figure 2 shows).

It is interesting to examine which way of reusing data can benefit the agent more. To answer this question, we compare SAC-SMR ($M = 10$) against SAC-UTD (UTD $G = 10$) and vanilla SAC on four DMC suite tasks. We run each algorithm for 1M online interactions. One can see that with the identical gradient steps per interaction with the environment, SMR achieves much better final performance and sample efficiency than UTD, as shown in Figure 9 and Table 2, indicating that SMR may be a better choice in practice. We remark here that the success of UTD in REDQ is attributed to a much higher UTD ratio and randomized critic ensemble. However, SMR does not rely on any specific component and can consistently improve the performance of the base algorithm. Meanwhile, we do not view SMR and UTD as contradictory methods, but rather orthogonal methods, e.g., one can find in Figure 4 that SMR improves the sample efficiency of REDQ.

7 Related Work

Off-policy RL algorithms. Recently, we have witnessed the great success of off-policy algorithms in discrete settings since DQN [67]. There are many improvements upon it, including double Q-learning [93, 94], dueling structure [98], distributional perspective [4, 69, 15], experience replay techniques [78, 40], self-supervised learning [53, 80, 84], model-based methods [45, 105, 79, 35, 39], etc.

In the continuous control domain, off-policy RL algorithms are widely adopted, such as DDPG [61] and TD3 [29]. These methods are usually built upon the actor-critic framework [75, 48], accompanied with a replay buffer for storing past experiences. There are also many efforts in exploring off-policy training with image input [27, 21, 81, 68, 55, 104, 32, 33, 106].

Sample-efficient continuous control algorithms. How to improve the sample efficiency is one of the most critical issues to deploying the RL algorithms widely in the real world. Existing work realizes it via adding exploration noise [61, 74], extra bonus reward [90, 28, 42, 1], multiple actors [107, 64], value estimate correction [72, 100, 50, 49, 65], or by leveraging maximum entropy framework [109, 30, 31], incorporating uncertainty measurement [56], etc. *SMR is orthogonal to all these advances* and can be easily combined with them.

Another line of research aiming at improving the sample efficiency in continuous control tasks sets their focus on learning a dynamics model of the environment [86, 9, 12, 44, 19, 57, 36, 97]. However, training an accurate model can be difficult [2, 3, 51] due to compounding errors [17, 95, 89], and it is very time-consuming to run model-based RL codebase.

Data replay methods. There are many ways of utilizing data in deep RL scenario, e.g., replaying good transitions [78, 62, 108, 46], balancing synthetic data and real data in model-based RL [37, 71], etc. Some studies [26, 20, 60] explore and uncover the advantages of update frequency on the collected transitions in a bootstrapping way for sample efficiency. SMR, instead, reuses the fixed batch data for multiple times to aid sample efficiency, and is orthogonal to previous methods.

8 Conclusion

In this paper, we propose sample multiple reuse (SMR), a novel method for enhancing the exploitation ability of off-policy continuous control RL algorithms by optimizing the agent on the fixed sampled batch multiple times. We show the convergence property of Q-learning with SMR in the tabular

case. SMR can be incorporated with *any* off-policy RL algorithms to boost their sample efficiency. We empirically show that the benefits of SMR are both algorithm-agnostic and task-agnostic. We further show that SMR is different from amplifying learning rate and discuss the potential overfitting phenomenon when using SMR. We hope this work can provide some insights to the community and aid the design of more advanced off-policy RL algorithms.

The main limitation of our work lies in the fact that injecting a sample reuse loop for training neural networks takes extra time. Such cost is negligible for state-based tasks but not for image-based tasks (check Appendix C). A promising solution may be dropout [85], which has been previously adopted to reduce the computation cost of REDQ in [41]. We leave it as future work.

References

- [1] J. Achiam and S. S. Sastry. Surprise-Based Intrinsic Motivation for Deep Reinforcement Learning. *ArXiv*, abs/1703.01732, 2017.
- [2] K. Asadi, E. Cater, D. K. Misra, and M. L. Littman. Towards a Simple Approach to Multi-step Model-based Reinforcement Learning. *ArXiv*, abs/1811.00128, 2018.
- [3] K. Asadi, D. K. Misra, and M. L. Littman. Lipschitz Continuity in Model-based Reinforcement Learning. In *International Conference on Machine Learning*, 2018.
- [4] M. G. Bellemare, W. Dabney, and R. Munos. A Distributional Perspective on Reinforcement Learning. In *International Conference on Machine Learning*, 2017.
- [5] M. G. Bellemare, Y. Naddaf, J. Veness, and M. Bowling. The Arcade Learning Environment: An Evaluation Platform for General Agents. In *International Joint Conference on Artificial Intelligence*, 2012.
- [6] D. Bertsekas. *Dynamic Programming and Optimal Control*, volume 1. Athena scientific, 1995.
- [7] L. Bottou. Large-Scale Machine Learning with Stochastic Gradient Descent. In *International Conference on Computational Statistics*, 2010.
- [8] G. Brockman, V. Cheung, L. Pettersson, J. Schneider, J. Schulman, J. Tang, and W. Zaremba. OpenAI Gym. *ArXiv*, abs/1606.01540, 2016.
- [9] J. Buckman, D. Hafner, G. Tucker, E. Brevdo, and H. Lee. Sample-Efficient Reinforcement Learning with Stochastic Ensemble Value Expansion. In *Advances in Neural Information Processing Systems (NeurIPS)*, 2018.
- [10] Y. Burda, H. Edwards, A. J. Storkey, and O. Klimov. Exploration by Random Network Distillation. *ArXiv*, abs/1810.12894, 2018.
- [11] X. Chen, C. Wang, Z. Zhou, and K. W. Ross. Randomized Ensembled Double Q-Learning: Learning Fast Without a Model. In *International Conference on Learning Representation*, 2021.
- [12] K. Chua, R. Calandra, R. McAllister, and S. Levine. Deep Reinforcement Learning in a Handful of Trials using Probabilistic Dynamics Models. In *Advances in Neural Information Processing Systems (NeurIPS)*, 2018.
- [13] C. Colas, O. Sigaud, and P.-Y. Oudeyer. GEP-PG: Decoupling Exploration and Exploitation in Deep Reinforcement Learning Algorithms. In *International Conference on Machine Learning*, 2017.
- [14] W. Dabney, Z. Kurth-Nelson, N. Uchida, C. K. Starkweather, D. Hassabis, R. Munos, and M. M. Botvinick. A Distributional Code for Value in Dopamine-based Reinforcement Learning. *Nature*, 577:671–675, 2020.
- [15] W. Dabney, M. Rowland, M. G. Bellemare, and R. Munos. Distributional Reinforcement Learning with Quantile Regression. In *AAAI Conference on Artificial Intelligence*, 2017.
- [16] J. Degraeve, F. Felici, J. Buchli, M. Neunert, B. D. Tracey, F. Carpanese, T. Ewalds, R. Hafner, A. Abdolmaleki, D. de Las Casas, C. Donner, L. Fritz, C. Galperti, A. Huber, J. Keeling, M. Tsimpoukelli, J. Kay, A. Merle, J.-M. Moret, S. Noury, F. Pesamosca, D. G. Pfau, O. Sauter, C. Sommariva, S. Coda, B. Duval, A. Fasoli, P. Kohli, K. Kavukcuoglu, D. Hassabis, and M. A. Riedmiller. Magnetic Control of Tokamak Plasmas through Deep Reinforcement Learning. *Nature*, 602:414 – 419, 2022.

- [17] M. P. Deisenroth and C. E. Rasmussen. PILCO: A Model-Based and Data-Efficient Approach to Policy Search. In *International Conference on Machine Learning*, 2011.
- [18] T. G. Dietterich. Overfitting and Undercomputing in Machine Learning. *ACM Computing Surveys*, 27:326–327, 1995.
- [19] P. D’Oro and W. Jaśkowski. How to Learn a Useful Critic? Model-based Action-Gradient-Estimator Policy Optimization. In *Advances in Neural Information Processing Systems*, 2020.
- [20] P. D’Oro, M. Schwarzer, E. Nikishin, P.-L. Bacon, M. G. Bellemare, and A. Courville. Sample-Efficient Reinforcement Learning by Breaking the Replay Ratio Barrier. In *Deep Reinforcement Learning Workshop NeurIPS 2022*, 2022.
- [21] D. Dwibedi, J. Tompson, C. Lynch, and P. Sermanet. Learning Actionable Representations from Visual Observations. *2018 IEEE/RSJ International Conference on Intelligent Robots and Systems (IROS)*, pages 1577–1584, 2018.
- [22] A. Ecoffet, J. Huizinga, J. Lehman, K. O. Stanley, and J. Clune. First Return, Then Explore. *Nature*, 590 7847:580–586, 2020.
- [23] B. Ellenberger. Pybullet gymperium. <https://github.com/benelot/pybullet-gym>, 2018.
- [24] E. Even-Dar and Y. Mansour. Learning Rates for Q-learning. *Journal of Machine Learning Research*, 5:1–25, 2004.
- [25] A. Fawzi, M. Balog, A. Huang, T. Hubert, B. Romera-Paredes, M. Barekatin, A. Novikov, F. J. R. Ruiz, J. Schrittwieser, G. Swirszcz, D. Silver, D. Hassabis, and P. Kohli. Discovering Faster Matrix Multiplication Algorithms with Reinforcement Learning. *Nature*, 610:47 – 53, 2022.
- [26] W. Fedus, P. Ramachandran, R. Agarwal, Y. Bengio, H. Larochelle, M. Rowland, and W. Dabney. Revisiting fundamentals of experience replay. In *International Conference on Machine Learning*, 2020.
- [27] C. Finn, X. Y. Tan, Y. Duan, T. Darrell, S. Levine, and P. Abbeel. Learning Visual Feature Spaces for Robotic Manipulation with Deep Spatial Autoencoders. *ArXiv*, abs/1509.06113, 2015.
- [28] J. Fu, J. D. Co-Reyes, and S. Levine. EX2: Exploration with Exemplar Models for Deep Reinforcement Learning. In *Advances in Neural Information Processing Systems*, 2017.
- [29] S. Fujimoto, H. van Hoof, and D. Meger. Addressing Function Approximation Error in Actor-Critic Methods. In *International Conference on Machine Learning (ICML)*, 2018.
- [30] T. Haarnoja, A. Zhou, P. Abbeel, and S. Levine. Soft Actor-Critic: Off-Policy Maximum Entropy Deep Reinforcement Learning with a Stochastic Actor. In *International Conference on Machine Learning (ICML)*, 2018.
- [31] T. Haarnoja, A. Zhou, K. Hartikainen, G. Tucker, S. Ha, J. Tan, V. Kumar, H. Zhu, A. Gupta, P. Abbeel, et al. Soft Actor-Critic Algorithms and Applications. *arXiv preprint arXiv:1812.05905*, 2018.
- [32] D. Hafner, T. Lillicrap, J. Ba, and M. Norouzi. Dream to Control: Learning Behaviors by Latent Imagination. In *International Conference on Learning Representations*, 2020.
- [33] D. Hafner, T. P. Lillicrap, I. S. Fischer, R. Villegas, D. R. Ha, H. Lee, and J. Davidson. Learning Latent Dynamics for Planning from Pixels. In *International Conference on Machine Learning*, 2018.
- [34] D. Hafner, T. P. Lillicrap, M. Norouzi, and J. Ba. Mastering Atari with Discrete World Models. In *International Conference on Learning Representations*, 2021.
- [35] J. B. Hamrick, A. L. Friesen, F. Behbahani, A. Guez, F. Viola, S. Witherspoon, T. Anthony, L. H. Buesing, P. Veličković, and T. Weber. On the role of planning in model-based deep reinforcement learning. In *International Conference on Learning Representations*, 2021.
- [36] N. Hansen, X. Wang, and H. Su. Temporal Difference Learning for Model Predictive Control. In *International Conference on Machine Learning*, 2022.
- [37] H. V. Hasselt, M. Hessel, and J. Aslanides. When to Use Parametric Models in Reinforcement Learning? In *Neural Information Processing Systems*, 2019.
- [38] P. Henderson, R. Islam, P. Bachman, J. Pineau, D. Precup, and D. Meger. Deep Reinforcement Learning that Matters. In *Proceedings of the AAAI conference on artificial intelligence*, 2018.

- [39] M. Hessel, I. Danihelka, F. Viola, A. Guez, S. Schmitt, L. Sifre, T. Weber, D. Silver, and H. V. Hasselt. Muesli: Combining Improvements in Policy Optimization. In *International Conference on Machine Learning*, 2021.
- [40] M. Hessel, J. Modayil, H. V. Hasselt, T. Schaul, G. Ostrovski, W. Dabney, D. Horgan, B. Piot, M. G. Azar, and D. Silver. Rainbow: Combining Improvements in Deep Reinforcement Learning. In *AAAI Conference on Artificial Intelligence*, 2017.
- [41] T. Hiraoka, T. Imagawa, T. Hashimoto, T. Onishi, and Y. Tsuruoka. Dropout Q-Functions for Doubly Efficient Reinforcement Learning. In *International Conference on Learning Representation*, 2022.
- [42] R. Houthoofd, X. Chen, Y. Duan, J. Schulman, F. D. Turck, and P. Abbeel. Curiosity-driven Exploration in Deep Reinforcement Learning via Bayesian Neural Networks. *ArXiv*, abs/1605.09674, 2016.
- [43] R. Islam, P. Henderson, M. Gomrokchi, and D. Precup. Reproducibility of Benchmarked Deep Reinforcement Learning Tasks for Continuous Control. *ArXiv*, abs/1708.04133, 2017.
- [44] M. Janner, J. Fu, M. Zhang, and S. Levine. When to Trust Your Model: Model-Based Policy Optimization. In *Advances in Neural Information Processing Systems (NeurIPS)*, 2019.
- [45] L. Kaiser, M. Babaeizadeh, P. Milos, B. Osinski, R. H. Campbell, K. Czechowski, D. Erhan, C. Finn, P. Kozakowski, S. Levine, A. Mohiuddin, R. Sepassi, G. Tucker, and H. Michalewski. Model-Based Reinforcement Learning for Atari. *ArXiv*, abs/1903.00374, 2019.
- [46] S. Kapturowski, G. Ostrovski, J. Quan, R. Munos, and W. Dabney. Recurrent Experience Replay in Distributed Reinforcement Learning. In *International Conference on Learning Representations*, 2018.
- [47] D. P. Kingma and J. Ba. Adam: A Method for Stochastic Optimization. In *International Conference on Learning Representation*, 2015.
- [48] V. R. Konda and J. N. Tsitsiklis. Actor-Critic Algorithms. In *Advances in Neural Information Processing Systems*, pages 1008–1014, 2000.
- [49] A. Kuznetsov, A. Grishin, A. Tsypin, A. Ashukha, and D. P. Vetrov. Automating Control of Overestimation Bias for Continuous Reinforcement Learning. *ArXiv*, abs/2110.13523, 2021.
- [50] A. Kuznetsov, P. Shvechikov, A. Grishin, and D. P. Vetrov. Controlling Overestimation Bias with Truncated Mixture of Continuous Distributional Quantile Critics. In *International Conference on Machine Learning*, 2020.
- [51] H. Lai, J. Shen, W. Zhang, and Y. Yu. Bidirectional Model-based Policy Optimization. In *International Conference on Machine Learning (ICML)*, 2020.
- [52] S. Lange, T. Gabel, and M. A. Riedmiller. Batch Reinforcement Learning. In *Reinforcement Learning*, 2012.
- [53] M. Laskin, K. Lee, A. Stooke, L. Pinto, P. Abbeel, and A. Srinivas. Reinforcement Learning with Augmented Data. In *Advances in Neural Information Processing Systems*, 2020.
- [54] Y. LeCun, Y. Bengio, and G. Hinton. Deep Learning. *Nature*, 521:436–444, 2015.
- [55] A. X. Lee, A. Nagabandi, P. Abbeel, and S. Levine. Stochastic Latent Actor-Critic: Deep Reinforcement Learning with a Latent Variable Model. In *Advances in Neural Information Processing Systems*, 2019.
- [56] K. Lee, M. Laskin, A. Srinivas, and P. Abbeel. SUNRISE: A Simple Unified Framework for Ensemble Learning in Deep Reinforcement Learning. In *International Conference on Machine Learning*, 2020.
- [57] C. Li, Y. Wang, W. Chen, Y. Liu, Z.-M. Ma, and T.-Y. Liu. Gradient Information Matters in Policy Optimization by Back-propagating through Model. In *International Conference on Learning Representations*, 2022.
- [58] G. Li, Ee, C. Cai, and Y. Wei. Is Q-Learning Minimax Optimal? A Tight Sample Complexity Analysis. *ArXiv*, abs/2102.06548, 2021.
- [59] G. Li, Y. Wei, Y. Chi, Y. Gu, and Y. Chen. Sample Complexity of Asynchronous Q-Learning: Sharper Analysis and Variance Reduction. *IEEE Transactions on Information Theory*, 68:448–473, 2020.
- [60] Q. Li, A. Kumar, I. Kostrikov, and S. Levine. Efficient Deep Reinforcement Learning Requires Regulating Overfitting. In *The Eleventh International Conference on Learning Representations*, 2023.

- [61] T. P. Lillicrap, J. J. Hunt, A. Pritzel, N. Heess, T. Erez, Y. Tassa, D. Silver, and D. Wierstra. Continuous Control with Deep Reinforcement Learning. In *International Conference on Learning Representation*, 2016.
- [62] X.-H. Liu, Z. Xue, J.-C. Pang, S. Jiang, F. Xu, and Y. Yu. Regret Minimization Experience Replay in Off-Policy Reinforcement Learning. In *Neural Information Processing Systems*, 2021.
- [63] I. Loshchilov and F. Hutter. SGDR: Stochastic Gradient Descent with Warm Restarts. In *International Conference on Learning Representations*, 2017.
- [64] J. Lyu, X. Ma, J. Yan, and X. Li. Efficient Continuous Control with Double Actors and Regularized Critics. In *Thirty-sixth AAAI Conference on Artificial Intelligence*, 2022.
- [65] J. Lyu, Y. Yang, J. Yan, and X. Li. Value Activation for Bias Alleviation: Generalized-activated Deep Double Deterministic Policy Gradients. *Neurocomputing*, 518:70–81, 2021.
- [66] F. S. Melo. Convergence of Q-learning: A Simple Proof. *Institute Of Systems and Robotics, Tech. Rep.*, pages 1–4, 2001.
- [67] V. Mnih, K. Kavukcuoglu, D. Silver, A. A. Rusu, J. Veness, M. G. Bellemare, A. Graves, M. A. Riedmiller, A. Fidjeland, G. Ostrovski, S. Petersen, C. Beattie, A. Sadik, I. Antonoglou, H. King, D. Kumaran, D. Wierstra, S. Legg, and D. Hassabis. Human-level Control through Deep Reinforcement Learning. *Nature*, 518:529–533, 2015.
- [68] A. Nair, V. H. Pong, M. Dalal, S. Bahl, S. Lin, and S. Levine. Visual Reinforcement Learning with Imagined Goals. In *Advances in Neural Information Processing Systems*, 2018.
- [69] D. W. Nam, Y. Kim, and C. Y. Park. GMAC: A Distributional Perspective on Actor-Critic Framework. In *International Conference on Machine Learning*, 2021.
- [70] E. Nikishin, M. Schwarzer, P. D’Oro, P.-L. Bacon, and A. C. Courville. The Primacy Bias in Deep Reinforcement Learning. In *International Conference on Machine Learning*, 2022.
- [71] F. Pan, J. He, D. Tu, and Q. He. Trust the Model When It Is Confident: Masked Model-based Actor-Critic. In *Advances in Neural Information Processing Systems*, 2020.
- [72] L. Pan, Q. Cai, and L. Huang. Softmax Deep Double Deterministic Policy Gradients. In *Advances in Neural Information Processing Systems*, 2020.
- [73] A. Paszke, S. Gross, F. Massa, A. Lerer, J. Bradbury, G. Chanan, T. Killeen, Z. Lin, N. Gimelshein, L. Antiga, A. Desmaison, A. Köpf, E. Yang, Z. DeVito, M. Raison, A. Tejani, S. Chilamkurthy, B. Steiner, L. Fang, J. Bai, and S. Chintala. PyTorch: An Imperative Style, High-Performance Deep Learning Library. In *Neural Information Processing Systems*, 2019.
- [74] M. Plappert, R. Houthoofd, P. Dhariwal, S. Sidor, R. Y. Chen, X. Chen, T. Asfour, P. Abbeel, and M. Andrychowicz. Parameter Space Noise for Exploration. *ArXiv*, abs/1706.01905, 2017.
- [75] D. V. Prokhorov and D. C. Wunsch. Adaptive Critic Designs. *IEEE Transactions on Neural Networks*, 8(5):997–1007, 1997.
- [76] G. Qu and A. Wierman. Finite-Time Analysis of Asynchronous Stochastic Approximation and Q-Learning. In *Annual Conference on Learning Theory*, 2020.
- [77] M. Sabry and A. M. A. Khalifa. On the Reduction of Variance and Overestimation of Deep Q-Learning. *ArXiv*, abs/1910.05983, 2019.
- [78] T. Schaul, J. Quan, I. Antonoglou, and D. Silver. Prioritized Experience Replay. *ArXiv*, abs/1511.05952, 2015.
- [79] J. Schrittwieser, I. Antonoglou, T. Hubert, K. Simonyan, L. Sifre, S. Schmitt, A. Guez, E. Lockhart, D. Hassabis, T. Graepel, T. P. Lillicrap, and D. Silver. Mastering Atari, Go, Chess and Shogi by Planning with a Learned Model. *Nature*, 588 7839:604–609, 2019.
- [80] M. Schwarzer, A. Anand, R. Goel, R. D. Hjelm, A. Courville, and P. Bachman. Data-Efficient Reinforcement Learning with Self-Predictive Representations. In *International Conference on Learning Representations*, 2021.
- [81] P. Sermanet, C. Lynch, Y. Chebotar, J. Hsu, E. Jang, S. Schaal, and S. Levine. Time-Contrastive Networks: Self-Supervised Learning from Video. *2018 IEEE International Conference on Robotics and Automation (ICRA)*, pages 1134–1141, 2017.

- [82] D. Silver, A. Huang, C. J. Maddison, A. Guez, L. Sifre, G. van den Driessche, J. Schrittwieser, I. Antonoglou, V. Panneershelvam, M. Lanctot, S. Dieleman, D. Grewe, J. Nham, N. Kalchbrenner, I. Sutskever, T. P. Lillicrap, M. Leach, K. Kavukcuoglu, T. Graepel, and D. Hassabis. Mastering the Game of Go with Deep Neural Networks and Tree Search. *Nature*, 529:484–489, 2016.
- [83] S. Singh, T. Jaakkola, M. L. Littman, and C. Szepesvari. Convergence Results for Single-Step On-Policy Reinforcement-Learning Algorithms. *Machine Learning*, 38:287–308, 2000.
- [84] A. Srinivas, M. Laskin, and P. Abbeel. CURL: Contrastive Unsupervised Representations for Reinforcement Learning. In *International Conference on Machine Learning*, 2020.
- [85] N. Srivastava, G. E. Hinton, A. Krizhevsky, I. Sutskever, and R. Salakhutdinov. Dropout: A Simple Way to Prevent Neural Networks from Overfitting. *Journal of Machine Learning Research*, 15:1929–1958, 2014.
- [86] R. S. Sutton. Dyna, an Integrated Architecture for Learning, Planning, and Reacting. *SIGART Bull.*, 2(4):160–163, 1991.
- [87] R. S. Sutton and A. G. Barto. *Reinforcement Learning: An Introduction*. MIT Press, 2018.
- [88] C. Szepesvari. The Asymptotic Convergence-Rate of Q-learning. In *Advances in Neural Information Processing Systems*, 1997.
- [89] E. Talvitie. Self-Correcting Models for Model-Based Reinforcement Learning. In *AAAI Conference on Artificial Intelligence*, 2016.
- [90] H. Tang, R. Houthoofd, D. Foote, A. Stooke, X. Chen, Y. Duan, J. Schulman, F. D. Turck, and P. Abbeel. #Exploration: A Study of Count-Based Exploration for Deep Reinforcement Learning. In *Advances in Neural Information Processing Systems*, 2017.
- [91] Y. Tassa, Y. Doron, A. Muldal, T. Erez, Y. Li, D. de Las Casas, D. Budden, A. Abdolmaleki, J. Merel, A. Lefrancq, T. P. Lillicrap, and M. A. Riedmiller. DeepMind Control Suite. *ArXiv*, abs/1801.00690, 2018.
- [92] E. Todorov, T. Erez, and Y. Tassa. MuJoCo: A Physics Engine for Model-based Control. *IEEE/RSJ International Conference on Intelligent Robots and Systems*, 2012.
- [93] H. van Hasselt. Double Q-learning. In *Advances in Neural Information Processing Systems*, 2010.
- [94] H. van Hasselt, A. Guez, and D. Silver. Deep Reinforcement Learning with Double Q-Learning. In *AAAI Conference on Artificial Intelligence*, 2015.
- [95] A. Venkatraman, M. Hebert, and J. A. Bagnell. Improving Multi-Step Prediction of Learned Time Series Models. In *AAAI Conference on Artificial Intelligence*, 2015.
- [96] O. Vinyals, I. Babuschkin, W. M. Czarnecki, M. Mathieu, A. Dudzik, J. Chung, D. H. Choi, R. Powell, T. Ewalds, P. Georgiev, J. Oh, D. Horgan, M. Kroiss, I. Danihelka, A. Huang, L. Sifre, T. Cai, J. P. Agapiou, M. Jaderberg, A. S. Vezhnevets, R. Leblond, T. Pohlen, V. Dalibard, D. Budden, Y. Sulsky, J. Molloy, T. L. Paine, C. Gulcehre, Z. Wang, T. Pfaff, Y. Wu, R. Ring, D. Yogatama, D. Wünsch, K. McKinney, O. Smith, T. Schaul, T. P. Lillicrap, K. Kavukcuoglu, D. Hassabis, C. Apps, and D. Silver. Grandmaster Level in StarCraft II using Multi-agent Reinforcement Learning. *Nature*, pages 1–5, 2019.
- [97] C. A. Voelcker, V. Liao, A. Garg, and A. massoud Farahmand. Value Gradient weighted Model-Based Reinforcement Learning. In *International Conference on Learning Representations*, 2022.
- [98] Z. Wang, T. Schaul, M. Hessel, H. V. Hasselt, M. Lanctot, and N. de Freitas. Dueling Network Architectures for Deep Reinforcement Learning. In *International Conference on Machine Learning*, 2016.
- [99] C. Watkins and P. Dayan. Q-learning. *Machine Learning*, 8:279–292, 1992.
- [100] D. Wu, X. Dong, J. Shen, and S. C. H. Hoi. Reducing Estimation Bias via Triplet-Average Deep Deterministic Policy Gradient. *IEEE Transactions on Neural Networks and Learning Systems*, 31:4933–4945, 2020.
- [101] Z. Wu, C. Yu, C. Chen, J. HAO, and H. H. Zhuo. Plan To Predict: Learning an Uncertainty-Foreseeing Model For Model-Based Reinforcement Learning. In A. H. Oh, A. Agarwal, D. Belgrave, and K. Cho, editors, *Advances in Neural Information Processing Systems*, 2022.

- [102] Z. Wu, C. Yu, C. Chen, H. Jianye, and H. H. Zhuo. Plan To Predict: Learning an Uncertainty-Foreseeing Model For Model-Based Reinforcement Learning. In *Advances in Neural Information Processing Systems*, 2022.
- [103] D. Yarats, R. Fergus, A. Lazaric, and L. Pinto. Mastering Visual Continuous Control: Improved Data-Augmented Reinforcement Learning. In *International Conference on Learning Representations*, 2022.
- [104] D. Yarats, I. Kostrikov, and R. Fergus. Image Augmentation Is All You Need: Regularizing Deep Reinforcement Learning from Pixels. In *International Conference on Learning Representations*, 2021.
- [105] W. Ye, S. Liu, T. Kurutach, P. Abbeel, and Y. Gao. Mastering Atari Games with Limited Data. In *Advances in Neural Information Processing Systems*, 2021.
- [106] Z. Yuan, Z. Xue, B. Yuan, X. Wang, Y. Wu, Y. Gao, and H. Xu. Pre-Trained Image Encoder for Generalizable Visual Reinforcement Learning. *ArXiv*, abs/2212.08860, 2022.
- [107] S. Zhang, H. Chen, and H. Yao. ACE: An Actor Ensemble Algorithm for Continuous Control with Tree Search. In *AAAI Conference on Artificial Intelligence*, 2018.
- [108] S. Zhang and R. S. Sutton. A Deeper Look at Experience Replay. *ArXiv*, abs/1712.01275, 2017.
- [109] B. D. Ziebart. *Modeling Purposeful Adaptive Behavior with the Principle of Maximum Causal Entropy*. Carnegie Mellon University, 2010.

A Additional Theoretical Results

In this section, we present additional theoretical results concerning on the sample complexity and finite time error bound for Q-SMR in nonreturnable MDPs. We first need to impose the following assumptions, which extends the assumption we made in the main text. All of the missing proofs can be found in Appendix B.

Assumption 2 (MDP Regularity). (1) $\forall t$, the reward signal is bounded, $|r_t| \leq r_{\max}$; (2) The Markov chain induced by the stationary behavior policy π_b is uniformly ergodic, and has a mixing time t_{mix} ,

$$t_{\text{mix}} := \min \left\{ t \mid \max_{(s_0, a_0) \in \mathcal{S} \times \mathcal{A}} D_{\text{TV}}(P^t(\cdot | s_0, a_0) \| \mu_{\pi_b}) \leq \frac{1}{4} \right\}.$$

$P^t(\cdot | s_0, a_0)$ is the distribution of (s_t, a_t) conditioned on the initial state-action pair (s_0, a_0) and $D_{\text{TV}}(p \| q)$ denotes the total variation distance between two distributions p, q . Denote μ_{π_b} as the stationary distribution of the aforementioned Markov chain. We define $\mu_{\min} := \inf_{(s, a) \in \mathcal{S} \times \mathcal{A}} \mu_{\pi_b}$.

We are now interested in the sample complexity of the Q-SMR algorithm, which is built upon Corollary 1. Note that a general analysis on the sample complexity of Q-SMR is very hard as the target value keeps changing during SMR iteration. We thus resort to nonreturnable MDP and present the sample complexity results in the appendix. We introduce an important lemma on the learning rate sequence in Lemma 1, which plays a critical role in proving Theorem 5.

Lemma 1. Denote $\hat{\alpha}_t = 1 - (1 - \alpha_t)^M$, then we have

$$\alpha_t \leq \hat{\alpha}_t \leq \min\{1, M\alpha_t\}. \quad (10)$$

We then formally present the sample complexity of Q-SMR.

Theorem 5 (Finite time error bound). Assume that Assumption 1 holds and the SMR ratio is set to be M . Suppose the learning rate is taken to be $\alpha_t = \frac{h}{M(t+t_0)}$ with $t_0 \geq \max(4h, \lceil \log_2 \frac{2}{\mu_{\min}} \rceil t_{\text{mix}})$ and $h \geq \frac{4}{\mu_{\min}(1-\gamma)}$, then with probability at least $1 - \delta$,

$$\|\hat{Q}_T - Q^*\|_{\infty} \leq \tilde{O} \left(\frac{r_{\max} \sqrt{t_{\text{mix}}}}{(1-\gamma)^{2.5} \mu_{\min} \sqrt{T}} + \frac{r_{\max} t_{\text{mix}}}{(1-\gamma)^3 \mu_{\min}^2 T} \right). \quad (11)$$

As an immediate corollary, we have:

Corollary 2 (Sample complexity). For any $0 < \delta < 1$ and $0 < \epsilon < 1$, with the Q-SMR algorithm we have:

$$\forall (s, a) \in \mathcal{S} \times \mathcal{A} : \|\hat{Q}_T - Q^*\|_{\infty} \leq \epsilon, \quad (12)$$

holds with probability at least $1 - \delta$, provided the iteration number T obeys:

$$T \gtrsim \frac{r_{\max}^2 t_{\text{mix}}}{(1-\gamma)^5 \mu_{\min}^2 \epsilon^2}. \quad (13)$$

Remark: The above conclusion says that the sample complexity of Q-SMR gives $\tilde{O} \left(\frac{t_{\text{mix}}}{(1-\gamma)^5 \mu_{\min}^2 \epsilon^2} \right)$. This result matches the recent theoretical analysis on the sample complexity of asynchronous Q-learning [76], which improves over the previous bound [88, 24]. For a detailed comparison, we notice that the above sample complexity becomes $\tilde{O} \left(\frac{t_{\text{mix}} (|\mathcal{S}||\mathcal{A}|)^2}{(1-\gamma)^5 \epsilon^2} \right)$ by using that $\frac{1}{\mu_{\min}}$ scales with $(|\mathcal{S}||\mathcal{A}|)$. The prior bound in [88] gives a sample complexity of $\tilde{O} \left(\frac{(|\mathcal{S}||\mathcal{A}|)^5}{(1-\gamma)^5 \epsilon^{2.5}} \right)$ ($\omega = 0.8$) and $\tilde{O} \left(\frac{(|\mathcal{S}||\mathcal{A}|)^{3.3}}{(1-\gamma)^{5.2} \epsilon^{2.6}} \right)$ ($\omega = 0.77$), where ω is the step size. Our results are sharper in terms of the dependence of $\frac{1}{1-\gamma}, \frac{1}{\epsilon}, (|\mathcal{S}||\mathcal{A}|)$. The result can be extended to a constant learning rate (i.e., $\alpha_t \equiv \alpha, \forall t$) by following a similar analysis as [59, 58].

B Missing Proofs

B.1 Proof of Theorem 1

Theorem 6. *The update rule of Q-SMR is equivalent to:*

$$\begin{aligned} Q_{t+1}(s_t, a_t) &= (1 - \alpha_t)^M Q_t(s_t, a_t) + \sum_{i=0}^{M-1} \alpha_t (1 - \alpha_t)^i \mathcal{T}_{t+1} Q_{t+1}^{(M-1-i)}(s_t, a_t), \\ Q_{t+1}(s, a) &= Q_t(s, a) \quad \forall (s, a) \neq (s_t, a_t), \end{aligned} \quad (14)$$

where $\mathcal{T}_{t+1} Q_{t+1}(s_t, a_t) = r_t + \gamma \max_{a' \in \mathcal{A}} Q_{t+1}(s_{t+1}, a')$ denotes the empirical Bellman operator w.r.t. timestep $t + 1$.

Proof. Note that we omit the superscript (M) for both the right $Q_t(s_t, a_t)$ and the left $Q_{t+1}(s_t, a_t)$ for clarity. We do M iterations in SMR with intermediate Q value labeled as $Q_t^{(i)}$ at timestep t and iteration $i, i \in \{1, 2, \dots, M\}$. Set the current Q -function at timestep t as $Q_t^{(0)}$, then with the SMR iteration, we have $Q_t^{(M)}(s_t, a_t)$ which is set to be the new Q -function at timestep $t + 1$, $Q_{t+1}^{(0)}(s_t, a_t) = Q_t^{(M)}(s_t, a_t)$. Note that in SMR iteration, the timestep is fixed, only the superscript changes with iteration, using the rule that $Q_{t+1}^{(i)}(s_t, a_t) = (1 - \alpha_t) Q_{t+1}^{(i-1)}(s_t, a_t) + \alpha_t \mathcal{T}_{t+1} Q_{t+1}^{(i-1)}(s_t, a_t), i \in \{1, 2, \dots, M\}$. Then run the loop till convergence. We will use induction to show the above conclusion.

If $M = 1$, then the update rule becomes the vanilla Q-learning style (notice that $Q_t^{(0)}(\cdot, \cdot) = Q_t(\cdot, \cdot)$).

Now for $\forall M \geq 1$, let us assume the update rule holds, if $(s, a) = (s_t, a_t)$, then,

$$Q_{t+1}^{(M)}(s_t, a_t) = (1 - \alpha_t)^M Q_{t+1}^{(0)}(s_t, a_t) + \sum_{i=0}^{M-1} \alpha_t (1 - \alpha_t)^i \mathcal{T}_{t+1} Q_{t+1}^{(M-1-i)}(s_t, a_t). \quad (15)$$

Thus,

$$\begin{aligned} Q_{t+1}^{(M+1)}(s_t, a_t) &= (1 - \alpha_t) Q_{t+1}^{(M)}(s_t, a_t) + \alpha_t \mathcal{T}_{t+1} Q_{t+1}^{(M)}(s_t, a_t). \quad (\text{By doing one iteration.}) \\ &= (1 - \alpha_t) \left[(1 - \alpha_t)^M Q_{t+1}^{(0)}(s_t, a_t) + \sum_{i=0}^{M-1} \alpha_t (1 - \alpha_t)^i \mathcal{T}_{t+1} Q_{t+1}^{(M-1-i)}(s_t, a_t) \right] + \alpha_t \mathcal{T}_{t+1} Q_{t+1}^{(M)}(s_t, a_t). \\ &= (1 - \alpha_t)^{M+1} Q_{t+1}^{(0)}(s_t, a_t) + \sum_{i=1}^M \alpha_t (1 - \alpha_t)^i \mathcal{T}_{t+1} Q_{t+1}^{(M-i)}(s_t, a_t) + \alpha_t \mathcal{T}_{t+1} Q_{t+1}^{(M)}(s_t, a_t). \\ &= (1 - \alpha_t)^{M+1} Q_{t+1}^{(0)}(s_t, a_t) + \sum_{i=0}^M \alpha_t (1 - \alpha_t)^i \mathcal{T}_{t+1} Q_{t+1}^{(M-i)}(s_t, a_t) \\ &= (1 - \alpha_t)^{M+1} Q_t^{(M+1)}(s_t, a_t) + \sum_{i=0}^M \alpha_t (1 - \alpha_t)^i \mathcal{T}_{t+1} Q_{t+1}^{(M-i)}(s_t, a_t) \end{aligned}$$

Then by induction and omitting the superscript $(M+1)$, we deduce that the update rule holds for $\forall M \geq 1$. \square

Remark: It is quite hard to trace back the intermediate Bellman backup $\mathcal{T}_{t+1} Q_{t+1}^{(i)}(s_t, a_t)$ since it is taken over $r_t + \gamma \max_{a' \in \mathcal{A}} Q_{t+1}^{(i)}(s_{t+1}, a')$. Though s_{t+1} is known, the maximal Q value may change position with the iteration.

B.2 Proof of Theorem 2

Theorem 7 (Stability). *Let Assumption 2 holds and assume that the initial Q -function is set to be 0, then for any iteration t , the value estimate induced by the Q-SMR, \hat{Q}_t , is bounded, i.e., $|\hat{Q}_t| \leq \frac{r_{\max}}{1 - \gamma}, \forall t$.*

Proof. We also show this by induction. Obviously, $|\hat{Q}_0| = 0 \leq \frac{r_{\max}}{1-\gamma}$. Now let us suppose for $\forall t \geq 0$, $|\hat{Q}_t| \leq \frac{r_{\max}}{1-\gamma}$, then by using the update rule from Theorem 1, we have

$$\begin{aligned}
|\hat{Q}_{t+1}(s_t, a_t)| &= \left| (1-\alpha_t)^M \hat{Q}_t(s_t, a_t) + \sum_{i=0}^{M-1} \alpha_t (1-\alpha_t)^i \mathcal{T}_{t+1} \hat{Q}_{t+1}^{(M-1-i)}(s_t, a_t) \right| \\
&= \left| (1-\alpha_t)^M \hat{Q}_t(s_t, a_t) + \sum_{i=0}^{M-1} \alpha_t (1-\alpha_t)^i \left[r_t + \gamma \max_{a' \in \mathcal{A}} \hat{Q}_{t+1}^{(M-1-i)}(s_{t+1}, a') \right] \right| \\
&\leq (1-\alpha_t)^M |\hat{Q}_t(s_t, a_t)| + \sum_{i=0}^{M-1} \alpha_t (1-\alpha_t)^i \left| r_t + \gamma \max_{a' \in \mathcal{A}} \hat{Q}_{t+1}^{(M-1-i)}(s_{t+1}, a') \right| \\
&\leq (1-\alpha_t)^M \frac{r_{\max}}{1-\gamma} + \sum_{i=0}^{M-1} \alpha_t (1-\alpha_t)^i \left[|r_t| + \gamma \max_{a' \in \mathcal{A}} |\hat{Q}_{t+1}^{(M-1-i)}(s_{t+1}, a')| \right] \\
&\leq (1-\alpha_t)^M \frac{r_{\max}}{1-\gamma} + \sum_{i=0}^{M-1} \alpha_t (1-\alpha_t)^i \left[r_{\max} + \gamma \frac{r_{\max}}{1-\gamma} \right] \\
&= (1-\alpha_t)^M \frac{r_{\max}}{1-\gamma} + \left[\sum_{i=0}^{M-1} \alpha_t (1-\alpha_t)^i \right] \frac{r_{\max}}{1-\gamma} \\
&= (1-\alpha_t)^M \frac{r_{\max}}{1-\gamma} + \left[1 - (1-\alpha_t)^M \right] \frac{r_{\max}}{1-\gamma} \\
&= \frac{r_{\max}}{1-\gamma}.
\end{aligned}$$

By using induction, we deduce that $\forall t \geq 0$ the Q-SMR outputs stable Q value, which satisfies $|\hat{Q}_t| \leq \frac{r_{\max}}{1-\gamma}$. \square

B.3 Proof of Corollary 1

Corollary 3. *If the MDP is nonreturnable, i.e., $s_{t+1} \neq s_t$, the update rule of Q-SMR gives:*

$$\begin{aligned}
Q_{t+1}(s_t, a_t) &= (1-\alpha_t)^M Q_t(s_t, a_t) + \left[1 - (1-\alpha_t)^M \right] \mathcal{T}_{t+1} Q_t(s_t, a_t), \\
Q_{t+1}(s, a) &= Q_t(s, a) \quad \forall (s, a) \neq (s_t, a_t),
\end{aligned} \tag{16}$$

Proof. If the MDP is nonreturnable, then it is easy to address the empirical Bellman backup $\mathcal{T}_{t+1} Q_{t+1}^{(i)}$. We have that $\mathcal{T}_{t+1} Q_{t+1}^{(i)}(s_t, a_t) = r_t + \gamma \max_{a' \in \mathcal{A}} Q_{t+1}^{(i)}(s_{t+1}, a')$. Since it is asynchronous Q-learning, only entry (s_t, a_t) will be updated inside the SMR loop. That is to say, $\mathcal{T}_{t+1} Q_{t+1}^{(i)}(s_t, a_t) = r_t + \gamma \max_{a' \in \mathcal{A}} Q_{t+1}^{(i)}(s_{t+1}, a')$ is unchanged throughout the SMR iteration. Therefore, based on Theorem 6, we have that the update rule gives

$$\begin{aligned}
Q_{t+1}(s_t, a_t) &= (1-\alpha_t)^M Q_t(s_t, a_t) + \sum_{i=0}^{M-1} \alpha_t (1-\alpha_t)^i \mathcal{T}_{t+1} Q_{t+1}^{(M-1-i)}(s_t, a_t), \\
&= (1-\alpha_t)^M Q_t(s_t, a_t) + \sum_{i=0}^{M-1} \alpha_t (1-\alpha_t)^i \mathcal{T}_{t+1} Q_t(s_t, a_t), \\
&= (1-\alpha_t)^M Q_t(s_t, a_t) + \left[1 - (1-\alpha_t)^M \right] \mathcal{T}_{t+1} Q_t(s_t, a_t).
\end{aligned}$$

\square

Remark: If we also let $s_{t+1} = s_t$ follow the above update rule, then the analysis below (e.g., sample complexity) can be extended naturally. This, however, triggers a gap between the original SMR loop and this practical update rule. We thus enforce $s_{t+1} \neq s_t$. Our analysis is restricted to nonreturnable MDPs, while our empirical results remedy this and validate the effectiveness of our proposed method.

B.4 Proof of Theorem 3

In order to show Theorem 3, we first present a well-known result from [83], which is built upon a proposition from [6].

Lemma 2. Consider a stochastic process $(\zeta_t, \Delta_t, F_t), t \geq 0$ where $\zeta_t, \Delta_t, F_t : X \mapsto \mathbb{R}$ satisfy the equation:

$$\Delta_{t+1}(x_t) = (1 - \zeta_t(x_t))\Delta_t(x_t) + \zeta_t(x_t)F_t(x_t), \quad (17)$$

where $x_t \in X$ and $t = 0, 1, 2, \dots$. Let P_t be a sequence of increasing σ -fields such that ζ_0 and Δ_0 are P_0 -measurable and ζ_t, Δ_t and F_{t-1} are P_t -measurable, $t = 1, 2, \dots$. Assume the following conditions hold: (1) The set X is finite; (2) $\zeta_t(x_t) \in [0, 1]$, $\sum_t \zeta_t(x_t) = \infty$, $\sum_t (\zeta_t(x_t))^2 < \infty$ with probability 1 and $\forall x \neq x_t : \zeta_t(x_t) = 0$; (3) $\|\mathbb{E}[F_t|P_t]\| \leq \kappa\|\Delta_t\| + c_t$, where $\|\cdot\|$ denotes maximum norm, $\kappa \in [0, 1]$ and c_t converges to 0 with probability 1; (4) $\text{Var}[F_t(x_t)|P_t] \leq C(1 + \|\Delta_t\|)^2$, where C is some constant. Then Δ_t converges to 0 with probability 1.

We also need the following lemma, which will be of great help.

Lemma 3. If the learning rates satisfy $\alpha_t(s, a) \in [0, 1]$, $\sum_t \alpha_t(s, a) = \infty$, $\sum_t (\alpha_t(s, a))^2 < \infty$ with probability 1, then the following holds with probability 1:

$$\sum_{i=0}^{M-1} \alpha_t(1 - \alpha_t)^i \in [0, 1], \quad \sum_t \sum_{i=0}^{M-1} \alpha_t(1 - \alpha_t)^i = \infty, \quad \sum_t \left(\sum_{i=0}^{M-1} \alpha_t(1 - \alpha_t)^i \right)^2 < \infty. \quad (18)$$

Proof. It is easy to find that $\sum_{i=0}^{M-1} \alpha_t(1 - \alpha_t)^i = 1 - (1 - \alpha_t)^M$. Since $\alpha_t \in [0, 1]$, we have $1 - \alpha_t \in [0, 1]$, $(1 - \alpha_t)^M \in [0, 1]$ and therefore $\sum_{i=0}^{M-1} \alpha_t(1 - \alpha_t)^i = 1 - (1 - \alpha_t)^M \in [0, 1]$.

Meanwhile, $1 - \alpha_t \geq (1 - \alpha_t)^M$, then $\sum_t \sum_{i=0}^{M-1} \alpha_t(1 - \alpha_t)^i \geq \sum_t \alpha_t = \infty$, thus $\sum_t \sum_{i=0}^{M-1} \alpha_t(1 - \alpha_t)^i = \infty$.

Finally, $\sum_t \left(\sum_{i=0}^{M-1} \alpha_t(1 - \alpha_t)^i \right)^2 \leq \sum_t \left(\sum_{i=0}^{M-1} \alpha_t \right)^2 = M^2 \sum_t (\alpha_t)^2 < \infty$. \square

Then we formally give the convergence property of Q-SMR below.

Theorem 8 (Formal, Convergence of Q-SMR). Given the following conditions: (1) each state-action pair is sampled an infinite number of times; (2) the MDP is finite; (3) $\gamma \in [0, 1]$; (4) Q values are stored in a look-up table; (5) the learning rates satisfy $\alpha_t(s, a) \in [0, 1]$, $\sum_t \alpha_t(s, a) = \infty$, $\sum_t (\alpha_t(s, a))^2 < \infty$ with probability 1 and $\alpha_t(s, a) \neq (s_t, a_t)$; (6) $\text{Var}[r(s, a)] < \infty, \forall s, a$, then the Q-SMR algorithm converges to the optimal Q-function.

Proof. To show the convergence of Q-SMR, we first show the convergence of the following update rule, which is exactly the rule of the simplified Q-SMR algorithm presented in the Corollary 1.

$$Q_{t+1}(s_t, a_t) = (1 - \alpha_t)^M Q_t(s_t, a_t) + \left[1 - (1 - \alpha_t)^M\right] \mathcal{T}_{t+1} Q_t(s_t, a_t). \quad (19)$$

Subtracting from both sides the quantity $Q^*(s_t, a_t)$, and letting $\Delta_t(s_t, a_t) = Q_t(s_t, a_t) - Q^*(s_t, a_t)$ yields:

$$\Delta_{t+1}(s_t, a_t) = (1 - \alpha_t)^M \Delta_t(s_t, a_t) + \left[1 - (1 - \alpha_t)^M\right] \left(r_t + \gamma \max_{a' \in \mathcal{A}} Q_t(s_{t+1}, a') - Q^*(s_t, a_t) \right).$$

Denote $\beta_t = 1 - (1 - \alpha_t)^M$, and write $F_t(s_t, a_t) = r_t + \gamma \max_{a' \in \mathcal{A}} Q_t(s_{t+1}, a') - Q^*(s_t, a_t)$, we have

$$\Delta_{t+1}(s_t, a_t) = (1 - \beta_t)\Delta_t(s_t, a_t) + \beta_t F_t.$$

From Lemma 3, we conclude that the new learning rate sequence obeys $\beta_t \in [0, 1]$, $\sum_t \beta_t = \infty$ and $\sum_t (\beta_t)^2 < \infty$. Meanwhile, $\mathbb{E}[F_t(s_t, a_t)|P_t] = \mathcal{T}Q_t(s_t, a_t) - Q^*(s_t, a_t)$. Since the optimal Q-function is a fixed point of the Bellman operator, we have $\mathbb{E}[F_t(s_t, a_t)|P_t] = \mathcal{T}Q_t(s_t, a_t) - \mathcal{T}Q^*(s_t, a_t)$. Since the Bellman operator is a contraction, we have $\|\mathbb{E}[F_t(s_t, a_t)|P_t]\| = \|\mathcal{T}Q_t(s_t, a_t) - \mathcal{T}Q^*(s_t, a_t)\| \leq \gamma\|\Delta_t\|$.

Finally, we check the variance of $F_t(s_t, a_t)$, it is easy to find:

$$\begin{aligned} \text{Var}[F_t(s_t, a_t)|P_t] &= \mathbb{E} \left[\left(r_t + \gamma \max_{a' \in \mathcal{A}} Q_t(s_{t+1}, a') - Q^*(s_t, a_t) - (\mathcal{T}Q_t(s_t, a_t) - Q^*(s_t, a_t)) \right)^2 \middle| P_t \right] \\ &= \mathbb{E} \left[\left(r_t + \gamma \max_{a' \in \mathcal{A}} Q_t(s_{t+1}, a') - \mathcal{T}Q_t(s_t, a_t) \right)^2 \middle| P_t \right] \\ &= \text{Var} \left[r_t + \gamma \max_{a' \in \mathcal{A}} Q_t(s_{t+1}, a') \middle| P_t \right]. \end{aligned}$$

Due to the fact that r_t is bounded, it clearly verifies that $\text{Var}[F_t(s_t, a_t)|P_t] \leq C(1 + \|\Delta_t\|)^2$ for some constant C . Combining these together, and by using Lemma 2, we conclude that Δ_t converges to 0 with probability

1. That is to say, the simplified Q-SMR algorithm with update rule in Equation 19 converges to the optimal Q -function. Then, for the formal Q-SMR update rule, we have

$$Q_{t+1}(s_t, a_t) = (1 - \alpha_t)^M Q_t(s_t, a_t) + \sum_{i=0}^{M-1} \alpha_t (1 - \alpha_t)^i \mathcal{T}_{t+1} Q_{t+1}^{(M-1-i)}(s_t, a_t) \quad (20)$$

$$\leq (1 - \alpha_t)^M Q_t(s_t, a_t) + \left[1 - (1 - \alpha_t)^M \right] \max_{i \in [0, M-1]} \mathcal{T}_{t+1} Q_t^{(i)}(s_t, a_t). \quad (21)$$

It is easy to check that the right side converges to the optimal Q -function by following the same analysis above. Furthermore, we have

$$Q_{t+1}(s_t, a_t) = (1 - \alpha_t)^M Q_t(s_t, a_t) + \sum_{i=0}^{M-1} \alpha_t (1 - \alpha_t)^i \mathcal{T}_{t+1} Q_{t+1}^{(M-1-i)}(s_t, a_t) \quad (22)$$

$$\geq (1 - \alpha_t)^M Q_t(s_t, a_t) + \left[1 - (1 - \alpha_t)^M \right] \min_{i \in [0, M-1]} \mathcal{T}_{t+1} Q_t^{(i)}(s_t, a_t). \quad (23)$$

Similarly, the lower bound side converges to the optimal Q -function. Then by combing the results above, we naturally conclude that Q-SMR converges to the optimal Q -function. \square

B.5 Proof of Theorem 4

Proof. If we amplify α_t , then we have

$$\theta_{t+1} = \theta_t - M\alpha_t \nabla \mathcal{L}_{\theta_t}. \quad (24)$$

This is the parameter update rule for the case of enlarging learning rate M times.

Now we investigate SMR with SGD. Denote $\theta_t^{(i)}$ as the intermediate parameter in the SMR loop at timestep t and iteration i , then it is easy to find $\theta_{t+1}^{(1)} = \theta_{t+1}^{(0)} - \alpha_t \nabla \mathcal{L}_{\theta_{t+1}^{(0)}}$, and $\theta_{t+1}^{(2)} = \theta_{t+1}^{(1)} - \alpha_t \nabla \mathcal{L}_{\theta_{t+1}^{(1)}} = \theta_{t+1}^{(0)} - \alpha_t \nabla \mathcal{L}_{\theta_{t+1}^{(0)}} - \alpha_t \nabla \mathcal{L}_{\theta_{t+1}^{(1)}}$. Finally, by doing iteration till M , using $\theta_{t+1}^{(0)} = \theta_t^{(M)}$ and omitting the superscript (M) , we have

$$\theta_{t+1} = \theta_t - \alpha_t \sum_{i=0}^{M-1} \nabla \mathcal{L}_{\theta_{t+1}^{(i)}}. \quad (25)$$

\square

B.6 Proof of Lemma 1

Lemma 4. Denote $\hat{\alpha}_t = 1 - (1 - \alpha_t)^M$, then we have

$$\alpha_t \leq \hat{\alpha}_t \leq \min\{1, M\alpha_t\}. \quad (26)$$

Proof. We write $f(x) = 1 - (1 - x)^M - x$ and $g(x) = 1 - (1 - x)^M - Mx$, $x \in [0, 1]$, $M \geq 1$, $M \in \mathbb{Z}$, then for $f(x)$, we have $f(x) = 1 - (1 - x)^M - x = (1 - x) - (1 - x)^M = (1 - x) [1 - (1 - x)^{M-1}] \geq 0$. Therefore, $1 - (1 - x)^M \geq x$.

For $g(x)$, we have

$$g'(x) = M(1 - x)^{M-1} - M = M \left[(1 - x)^{M-1} - 1 \right] \leq 0.$$

It indicates that $g(x)$ decreases in the region $[0, 1]$, thus $g(x) \leq g(0) = 0$ which incurs $1 - (1 - x)^M \leq Mx$, $\forall x \in [0, 1]$. Meanwhile, as $1 - (1 - x)^M \leq 1$, we thus have $1 - (1 - x)^M \leq \min\{1, Mx\}$.

By setting $x = \alpha_t$, we have the desired conclusions immediately. \square

B.7 Proof of Theorem 5

Theorem 9 (Finite time error bound). Assume that Assumption 1 holds and the SMR ratio is set to be M . Suppose the learning rate is taken to be $\alpha_t = \frac{h}{M(t+t_0)}$ with $t_0 \geq \max(4h, \lceil \log_2 \frac{2}{\mu_{\min}} \rceil t_{\text{mix}})$ and $h \geq \frac{4}{\mu_{\min}(1-\gamma)}$, then with probability at least $1 - \delta$,

$$\|\hat{Q}_T - Q^*\|_{\infty} \leq \tilde{\mathcal{O}} \left(\frac{r_{\max} \sqrt{t_{\text{mix}}}}{(1-\gamma)^{2.5} \mu_{\min}} \frac{1}{\sqrt{T}} + \frac{r_{\max} t_{\text{mix}}}{(1-\gamma)^3 \mu_{\min}^2} \frac{1}{T} \right) \quad (27)$$

The proof of this theorem is borrowed heavily from [76]. Throughout the proof, we denote $\|\cdot\|$ as the infinity norm. We also assume there exist some constant $C > 0$ s.t. $\|F(x)\| \leq \gamma\|x\| + C, \forall x \in \mathbb{R}^n$, where $F(\cdot)$ denotes the bellman operator. This assumption can be generally satisfied with $C = (1 + \gamma)\|x^*\|$ since $\|F(x)\| \leq \|F(x) - F(x^*)\| + \|F(x^*)\| \leq \gamma\|x - x^*\| + \|x^*\| \leq \gamma\|x\| + (1 + \gamma)\|x^*\|$.

Proof. The proof is generally divided into three steps. First, we decompose the error in a recursive form. Second, we bound the contribution of the noise sequence to the error decomposition. Third, we use the error decomposition and the bounds to prove the result. We let $\hat{\alpha}_t = 1 - (1 - \alpha_t)^M$ and rewrite the update rule for Q-SMR below.

$$\begin{aligned} x_i(t+1) &= x_i(t) + \hat{\alpha}_t(F_i(x(t)) - x_i(t) + \omega(t)), i = i_t, \\ x_i(t+1) &= x_i(t), i \neq i_t, \end{aligned}$$

where we write $Q_t(s_t, a_t)$ as $x_i(t)$, $i_t \in \{1, 2, \dots, n\}$ is a stochastic process adapted to a filtration P_t , $F_i(x(t)) = r(s_t, a_t) + \gamma \mathbb{E}_{s' \sim P(\cdot | s_t, a_t)} \max_{a' \in \mathcal{A}} Q_t(s', a')$, $\omega(t) = r_t + \gamma \max_{a' \in \mathcal{A}} Q_t(s_{t+1}, a') - r(s_t, a_t) - \gamma \mathbb{E}_{s' \sim P(\cdot | s_t, a_t)} \max_{a' \in \mathcal{A}} Q_t(s', a')$.

Following the same way in [76] (Equation 7), we rewrite the update formula as follows:

$$x(t+1) = (I - \hat{\alpha}_t D_t)x(t) + \hat{\alpha}_t D_t F(x(t)) + \hat{\alpha}_t(\epsilon(t) + \phi(t)),$$

where $\epsilon(t) = [(e_{i_t} e_{i_t}^T - D_t)(F(x(t-\tau)) - x(t-\tau)) + \omega(t)e_{i_t}]$, and e_i is the unit vector with its i -th entry 1 and others 0. Clearly, $x(t)$ is P_t measurable, and as $\epsilon(t)$ depends on $\omega(t)$ which is P_{t+1} measurable, $\epsilon(t)$ is P_{t+1} measurable. Moreover, we have

$$\mathbb{E}\epsilon(t)|P_{t-\tau} = \mathbb{E}[(e_{i_t} e_{i_t}^T - D_t)|P_{t-\tau}][F(x(t-\tau)) - x(t-\tau)] + \mathbb{E}[\mathbb{E}[\omega(t)|P_t]e_{i_t}|P_{t-\tau}] = 0, \quad (28)$$

where $D_t = \mathbb{E}e_{i_t} e_{i_t}^T | P_{t-\tau}$, τ is a positive integer. Assume there exist τ and a $\sigma' \in (0, 1)$ such that for any $i \in \mathcal{N}$, $\mathcal{N} = \{1, 2, \dots, n\}$ and $t \geq \tau$, $P(i_t = i | P_{t-\tau}) \geq \sigma' = M\sigma$, i.e., exploration is sufficient. Such requirement can be satisfied if we take $\sigma = \frac{1}{2}\mu_{\min}$ and $\tau = \lceil \log_2(\frac{2}{\mu_{\min}}) \rceil t_{\text{mix}}$ where $\lceil \cdot \rceil$ denotes taking ceiling of the integer, e.g., $\lceil 2.7 \rceil = 3$, $\lceil 5.1 \rceil = 6$. $\phi(t) = [(e_{i_t} e_{i_t}^T - D_t)(F(x(t)) - F(x(t-\tau)) - (x(t) - x(t-\tau)))]$.

We expand it recursively and have:

$$x(t+1) = \tilde{B}_{\tau-1,t}x(\tau) + \sum_{k=\tau}^t B_{k,t}F(x(k)) + \sum_{k=\tau}^t \hat{\alpha}_k \tilde{B}_{k,t}(\epsilon(k) + \phi(k)),$$

where $B_{k,t} = \hat{\alpha}_k D_k \prod_{l=k+1}^t (I - \hat{\alpha}_l D_l)$, $\tilde{B}_{k,t} = \prod_{l=k+1}^t (I - \hat{\alpha}_l D_l)$. It is easy to notice that $B_{k,t}$ and $\tilde{B}_{k,t}$ are n -by- n diagonal random metrics, with their i -th diagonal entry given by $b_{k,t,i} = \hat{\alpha}_k d_{k,i} \prod_{l=k+1}^t (1 - \hat{\alpha}_l d_{l,i})$ and $\tilde{b}_{k,t,i} = \prod_{l=k+1}^t (1 - \hat{\alpha}_l d_{l,i})$. For any i , the following holds almost surely,

$$b_{k,t,i} \leq \beta_{k,t} := \hat{\alpha}_k \prod_{l=k+1}^t (1 - \hat{\alpha}_l M\sigma), \quad \tilde{b}_{k,t,i} \leq \tilde{\beta}_{k,t} := \prod_{l=k+1}^t (1 - \hat{\alpha}_l M\sigma).$$

Based on Lemma 8 in [76], denote $a_t = \|x(t) - x^*\|$, then we have almost surely,

$$a_{t+1} \leq \tilde{\beta}_{\tau-1,t} a_\tau + \gamma \sup_{i \in \mathcal{N}} \sum_{k=\tau}^t b_{k,t,i} a_k + \left\| \sum_{k=\tau}^t \hat{\alpha}_k \tilde{B}_{k,t} \epsilon(k) \right\| + \left\| \sum_{k=\tau}^t \hat{\alpha}_k \tilde{B}_{k,t} \phi(k) \right\|. \quad (29)$$

Lemma 5. *The following bounds hold almost surely: (a) $\|\epsilon(t)\| \leq \bar{\epsilon} := \frac{4r_{\max}}{1-\gamma} + C$; (b) $\|\phi(t)\| \leq \sum_{k=t-\tau+1}^t 2\bar{\epsilon}\hat{\alpha}_{k-1}$.*

Proof. Replacing \bar{x} with $\frac{r_{\max}}{1-\gamma}$, $\bar{\omega}$ with $\frac{2r_{\max}}{1-\gamma}$ and using \underline{v} as 1 (since we use infinity norm), and replacing α_{k-1} with $\hat{\alpha}_{k-1}$ in Lemma 9 of [76] will induce the conclusion immediately. \square

These are still not enough to bound $\|\sum_{k=\tau}^t \hat{\alpha}_k \tilde{B}_{k,t} \epsilon(k)\|$ and $\|\sum_{k=\tau}^t \hat{\alpha}_k \tilde{B}_{k,t} \phi(k)\|$. We provide in the following lemma some useful results of $\beta_{k,t}$ and $\tilde{\beta}_{k,t}$.

Lemma 6. *If $\alpha_t = \frac{h}{M(t+t_0)}$, where $h > \frac{2}{\sigma}$ and $t_0 \geq \max(4h, \tau)$, then $\beta_{k,t}$ and $\tilde{\beta}_{k,t}$ satisfy the following relationships:*

$$\begin{aligned} (a) \quad \beta_{k,t} &\leq \frac{h}{k+t_0} \left(\frac{k+1+t_0}{t+1+t_0} \right)^{\sigma h}, \quad \tilde{\beta}_{k,t} \leq \left(\frac{k+1+t_0}{t+1+t_0} \right)^{\sigma h}; \quad (b) \quad \sum_{k=1}^t \beta_{k,t}^2 \leq \frac{2h}{\sigma} \frac{1}{t+1+t_0}; \\ (c) \quad \sum_{k=\tau}^t \beta_{k,t} \sum_{l=k-\tau+1}^k \hat{\alpha}_{l-1} &< \frac{8h\tau}{\sigma} \frac{1}{t+1+t_0}. \end{aligned}$$

Proof. For part (a), notice that $\log(1-x) \leq -x, \forall x < 1$, then

$$(1 - M\sigma\hat{\alpha}_t) \leq (1 - M\sigma\alpha_t) = e^{\log(1 - \frac{\sigma h}{t+t_0})} \leq e^{-\frac{\sigma h}{t+t_0}},$$

where we use $\hat{\alpha}_t \geq \alpha_t$ according to Lemma 4. Therefore, we have

$$\prod_{l=k+1}^t (1 - M\sigma\hat{\alpha}_l) \leq e^{-\sum_{l=k+1}^t \frac{\sigma h}{l+t_0}} \leq e^{-\int_{k+1}^{t+1} \frac{\sigma h}{y+t_0} dy} = e^{-\sigma h \log(\frac{t+1+t_0}{k+1+t_0})} = \left(\frac{k+1+t_0}{t+1+t_0}\right)^{\sigma h}.$$

This directly leads to the bound on $\tilde{\beta}_{k,t}$. We have $\beta_{k,t} = \hat{\alpha}_k \prod_{l=k+1}^t (1 - \hat{\alpha}_l \sigma) \leq M \frac{h}{M(k+t_0)} \left(\frac{k+1+t_0}{t+1+t_0}\right)^{\sigma h} = \frac{h}{k+t_0} \left(\frac{k+1+t_0}{t+1+t_0}\right)^{\sigma h}$, where we use the fact that $\hat{\alpha}_k \leq M\alpha_k$ based on Lemma 4.

For part (b), we have

$$\beta_{k,t}^2 \leq \frac{h^2}{(k+t_0)^2} \left(\frac{k+1+t_0}{t+1+t_0}\right)^{2\sigma h} = \frac{h^2}{(t+1+t_0)^{2\sigma h}} \frac{(k+1+t_0)^{2\sigma h}}{(k+t_0)^2} \leq \frac{2h^2}{(t+1+t_0)^{2\sigma h}} (k+t_0)^{2\sigma h-2},$$

where we have used $(k+1+t_0)^{2\sigma h} \leq 2(k+t_0)^{2\sigma h}$, which is true when $t_0 \geq 4h$. Then, we have

$$\begin{aligned} \sum_{k=1}^t \beta_{k,t}^2 &\leq \frac{2h^2}{(t+1+t_0)^{2\sigma h}} \sum_{k=1}^t (k+t_0)^{2\sigma h-2} \leq \frac{2h^2}{(t+1+t_0)^{2\sigma h}} \int_1^{t+1} (y+t_0)^{2\sigma h-2} dy \\ &< \frac{2h^2}{(t+1+t_0)^{2\sigma h}} \frac{1}{2\sigma h-1} (t+1+t_0)^{2\sigma h-1} < \frac{2h}{\sigma} \frac{1}{t+1+t_0}, \end{aligned}$$

where we have used the fact that $2\sigma h - 1 > \sigma h$ (as $h > \frac{2}{\sigma}$).

For part (c), notice that for $k - \tau \leq l \leq k - 1$ where $k \geq \tau$, we have $\alpha_l \leq \frac{h}{M(k - \tau + t_0)}$. Since $k \geq \tau$ and $t_0 > \max(4h, \tau)$ (the assumption), then we have $k + t_0 > 2\tau$ which indicates that $kh - 2h\tau + ht_0 > 0$, and thus $kh + ht_0 < 2kh - 2h\tau + 2ht_0$, which is to say $\frac{h}{k - \tau + t_0} < \frac{2h}{k + t_0}$. Therefore, we have $\alpha_l < \frac{2h}{M(k + t_0)}$.

By using Lemma 4, we have $\hat{\alpha}_l \leq M\alpha_l < \frac{2h}{k + t_0}$.

Then, we have

$$\begin{aligned} \sum_{k=\tau}^t \beta_{k,t} \sum_{l=k-\tau+1}^k \hat{\alpha}_{l-1} &< \sum_{k=\tau}^t \beta_{k,t} \frac{2h\tau}{k+t_0} \leq \sum_{k=\tau}^t \frac{h}{k+t_0} \left(\frac{k+1+t_0}{t+1+t_0}\right)^{\sigma h} \frac{2h\tau}{k+t_0} \leq \sum_{k=\tau}^t \frac{4h^2\tau}{(t+1+t_0)^{\sigma h}} (k+t_0)^{\sigma h-2} \\ &\leq \frac{4h^2\tau}{(t+1+t_0)^{\sigma h}} \int_{\tau}^{t+1} (y+t_0)^{\sigma h-2} dy \leq \frac{4h^2\tau}{(t+1+t_0)^{\sigma h}} \frac{(t+1+t_0)^{\sigma h-1}}{\sigma h-1} \\ &\leq \frac{8h\tau}{\sigma} \frac{1}{t+1+t_0}, \end{aligned}$$

where we have used $(k+1+t_0)^{\sigma h} \leq 2(k+t_0)^{\sigma h}$ and $\sigma h - 1 > \frac{1}{2}\sigma h$. \square

Now we are ready to bound $\|\sum_{k=\tau}^t \hat{\alpha}_k \tilde{B}_{k,t} \phi(k)\|$. It is easy to find that

$$\left\| \sum_{k=\tau}^t \hat{\alpha}_k \tilde{B}_{k,t} \phi(k) \right\| \leq \sum_{k=\tau}^t \hat{\alpha}_k \|\tilde{B}_{k,t}\| \|\phi(k)\| \leq \sum_{k=\tau}^t \beta_{k,t} \sum_{l=k-\tau+1}^k 2\bar{\epsilon} \hat{\alpha}_{l-1} < \frac{16\bar{\epsilon}h\tau}{\sigma(t+1+t_0)} := C_\phi \frac{1}{t+1+t_0},$$

where we have used the fact that each entry of $\tilde{B}_{k,t}$ is upper bounded by $\tilde{\beta}_{k,t}$, i.e., $\|\tilde{B}_{k,t}\| \leq \tilde{\beta}_{k,t}$ and $\beta_{k,t} = \hat{\alpha}_k \tilde{\beta}_{k,t}$ by definition. We now move on to bound $\|\sum_{k=\tau}^t \hat{\alpha}_k \tilde{B}_{k,t} \epsilon(k)\|$. It is straightforward that we use Azuma Hoeffding inequality to show this, which is presented in the following lemma.

Lemma 7 (Lemma 13 in [76]). *Let X_t be a P_t -adapted stochastic process with $\mathbb{E}X_t | P_{t-\tau} = 0$. Meanwhile, $|X_t| \leq \bar{X}_t$ almost surely, then with probability at least $1 - \delta$, we have $|\sum_{k=0}^t X_k| \leq \sqrt{2\tau \sum_{k=0}^t \bar{X}_k^2 \log(\frac{2\tau}{\delta})}$.*

Recall that $\sum_{k=\tau}^t \hat{\alpha}_k \tilde{B}_{k,t} \epsilon(k)$ is a random vector with its i -th entry $\sum_{k=\tau}^t \hat{\alpha}_k \epsilon_i(k) \prod_{l=k+1}^t (1 - \hat{\alpha}_l d_{l,i})$, $d_{l,i} \geq \sigma' = M\sigma$. Fixing i , $\epsilon_i(k)$ is a P_{k+1} adapted stochastic process satisfying $\mathbb{E}\epsilon_i(k) | P_{k-\tau} = 0$ (see Equation 28). However, $\prod_{l=k+1}^t (1 - \hat{\alpha}_l d_{l,i})$ is not $P_{k-\tau}$ measurable. To erase the randomness in it, we introduce the following lemma.

Lemma 8 (Adapted from Lemma 14 in [76]). *For each i , we have almost surely,*

$$\left| \sum_{k=\tau}^t \hat{\alpha}_k \epsilon_i(k) \prod_{l=k+1}^t (1 - \hat{\alpha}_l d_{l,i}) \right| \leq \sup_{\tau \leq k_0 \leq t} \left(\left| \sum_{k=k_0+1}^t \epsilon_i(k) \beta_{k,t} \right| + 2\bar{\epsilon} \beta_{k_0,t} \right).$$

Proof. Replacing α_k with $\hat{\alpha}_k$ and setting $v_i = 1$ (since we use standard infinity norm) in Lemma 14 of [76] conclude the proof. \square

After that, we can proceed with the proof with the aid of the following lemma.

Lemma 9. *For each t , with probability at least $1 - \delta$, we have*

$$\left\| \sum_{k=\tau}^t \hat{\alpha}_k \tilde{B}_{k,t} \epsilon(k) \right\| \leq 6\bar{\epsilon} \sqrt{\frac{(\tau+1)h}{\sigma(t+1+t_0)} \log \left(\frac{2(\tau+1)tn}{\delta} \right)}.$$

Proof. Fix i and $\tau \leq k_0 \leq t$, we have $\epsilon_i(k) \beta_{k,t}$ is a P_{k+1} adapted stochastic process satisfying $\mathbb{E} \epsilon_i(k) \beta_{k,t} | P_{k-\tau} = 0$. We also have $|\epsilon_i(k) \beta_{k,t}| \leq |\epsilon_i(k)| \beta_{k,t} \leq \bar{\epsilon} \beta_{k,t}$ (by using Lemma 5). We then can use the Azuma-Hoeffding bound in Lemma 8. With probability at least $1 - \delta$, we have

$$\left| \sum_{k=k_0+1}^t \epsilon_i(k) \beta_{k,t} \right| \leq \bar{\epsilon} \sqrt{2(\tau+1) \sum_{k=k_0+1}^t \beta_{k,t}^2 \log \left(\frac{2(\tau+1)}{\delta} \right)}.$$

By a union bound on $\tau \leq k_0 \leq t$, we have with probability at least $1 - \delta$,

$$\sup_{\tau \leq k_0 \leq t} \left| \sum_{k=k_0+1}^t \epsilon_i(k) \beta_{k,t} \right| \leq \bar{\epsilon} \sqrt{2(\tau+1) \sum_{k=\tau+1}^t \beta_{k,t}^2 \log \left(\frac{2(\tau+1)t}{\delta} \right)}.$$

Notice that $\sigma h > 2$ and hence $\frac{(k_0+1+t_0)^{\sigma h}}{k_0+t_0}$ monotonically increases with k_0 . Therefore, we have $\frac{(k_0+1+t_0)^{\sigma h}}{k_0+t_0} \leq \frac{(t+1+t_0)^{\sigma h}}{t+t_0}$, $\forall \tau \leq k_0 \leq t$. Here, we assume that $h > \frac{2}{\sigma(1-\gamma)}$ (again, we set $\sigma = \frac{1}{2} \mu_{\min}$) which obviously satisfies the assumption that $h > \frac{2}{\sigma}$ we make in Lemma 6.

Then, by using Lemma 8 and Lemma 6, we have with probability at least $1 - \delta$,

$$\begin{aligned} \left| \sum_{k=\tau}^t \hat{\alpha}_k \epsilon_i(k) \prod_{l=k+1}^t (1 - \hat{\alpha}_l d_{l,i}) \right| &\leq \sup_{\tau \leq k_0 \leq t} \left(\left| \sum_{k=k_0+1}^t \epsilon_i(k) \beta_{k,t} \right| + 2\bar{\epsilon} \beta_{k_0,t} \right) \\ &\leq \bar{\epsilon} \sqrt{2(\tau+1) \sum_{k=\tau+1}^t \beta_{k,t}^2 \log \left(\frac{2(\tau+1)t}{\delta} \right)} + \sup_{\tau \leq k_0 \leq t} 2\bar{\epsilon} \beta_{k_0,t} \\ &\leq 2\bar{\epsilon} \sqrt{\frac{(\tau+1)h}{\sigma(t+1+t_0)} \log \left(\frac{2(\tau+1)t}{\delta} \right)} + 2\bar{\epsilon} \sup_{\tau \leq k_0 \leq t} \frac{h}{k_0+t_0} \left(\frac{k_0+1+t_0}{t+1+t_0} \right)^{\sigma h} \\ &\leq 2\bar{\epsilon} \sqrt{\frac{(\tau+1)h}{\sigma(t+1+t_0)} \log \left(\frac{2(\tau+1)t}{\delta} \right)} + 2\bar{\epsilon} \frac{h}{t+t_0} \\ &\leq 6\bar{\epsilon} \sqrt{\frac{(\tau+1)h}{\sigma(t+1+t_0)} \log \left(\frac{2(\tau+1)t}{\delta} \right)}. \end{aligned}$$

The last inequality is due to that $\frac{1}{t+t_0}$ is asymptotically smaller than $\sqrt{\frac{1}{t+1+t_0}}$. Finally, by using the union bound over $i \in \{1, 2, \dots, n\}$, we have

$$\left| \sum_{k=\tau}^t \hat{\alpha}_k \epsilon_i(k) \prod_{l=k+1}^t (1 - \hat{\alpha}_l d_{l,i}) \right| \leq 6\bar{\epsilon} \sqrt{\frac{(\tau+1)h}{\sigma(t+1+t_0)} \log \left(\frac{2(\tau+1)tn}{\delta} \right)}.$$

\square

By replacing δ with $\frac{\delta}{t}$, we can rewrite the conclusion in Lemma 9 as:

$$\left\| \sum_{k=\tau}^t \hat{\alpha}_k \tilde{B}_{k,t} \epsilon(k) \right\| \leq 6\bar{\epsilon} \sqrt{\frac{(\tau+1)h}{\sigma(t+1+t_0)} \log \left(\frac{2(\tau+1)t^2 n}{\delta} \right)} := C_\epsilon \sqrt{\frac{1}{t+1+t_0}},$$

where $C_\epsilon = 6\bar{\epsilon} \sqrt{\frac{(\tau+1)h}{\sigma} \log \left(\frac{2(\tau+1)t^2 n}{\delta} \right)}$, then by recalling Equation 29, we have for $\tau \leq t \leq T$, with probability at least $1 - \delta$,

$$\begin{aligned} a_{t+1} &\leq \tilde{\beta}_{\tau-1,t} a_\tau + \gamma \sup_{i \in \mathcal{N}} \sum_{k=\tau}^t b_{k,t,i} a_k + \left\| \sum_{k=\tau}^t \hat{\alpha}_k \tilde{B}_{k,t} \epsilon(k) \right\| + \left\| \sum_{k=\tau}^t \hat{\alpha}_k \tilde{B}_{k,t} \phi(k) \right\| \\ &\leq \tilde{\beta}_{\tau-1,t} a_\tau + \gamma \sup_{i \in \mathcal{N}} \sum_{k=\tau}^t b_{k,t,i} a_k + \frac{C_\epsilon}{\sqrt{t+1+t_0}} + \frac{C_\phi}{t+1+t_0}. \end{aligned}$$

We now want to show that

$$a_T \leq \frac{C_a}{\sqrt{T+t_0}} + \frac{C'_a}{T+t_0}, \quad (30)$$

where $C_a = \frac{12\bar{\epsilon}}{1-\gamma} \sqrt{\frac{(\tau+1)h}{\sigma} \log \left(\frac{2(\tau+1)T^2 n}{\delta} \right)}$, $C'_a = \frac{4}{1-\gamma} \max(C_\phi, \frac{2(\tau+t_0)r_{\max}}{1-\gamma})$. We use induction to show

Equation 30. It is easy to see that when $t = \tau$, Equation 30 holds as $\frac{C'_a}{\tau+t_0} \geq \frac{8r_{\max}}{(1-\gamma)^2} \geq a_\tau$, where $a_\tau = \|x(\tau) - x^*\| \leq \|x(\tau)\| + \|x^*\| \leq \frac{2r_{\max}}{1-\gamma}$. We then assume that Equation 30 holds for up to $k \leq t$, then we have

$$\begin{aligned} a_{t+1} &\leq \tilde{\beta}_{\tau-1,t} a_\tau + \gamma \sup_{i \in \mathcal{N}} \sum_{k=\tau}^t b_{k,t,i} a_k + \frac{C_\epsilon}{\sqrt{t+1+t_0}} + \frac{C_\phi}{t+1+t_0} \\ &\leq \tilde{\beta}_{\tau-1,t} a_\tau + \gamma \sup_{i \in \mathcal{N}} \sum_{k=\tau}^t b_{k,t,i} \left(\frac{C_a}{\sqrt{k+t_0}} + \frac{C'_a}{k+t_0} \right) + \frac{C_\epsilon}{\sqrt{t+1+t_0}} + \frac{C_\phi}{t+1+t_0} \\ &= \tilde{\beta}_{\tau-1,t} a_\tau + \gamma \sup_{i \in \mathcal{N}} \sum_{k=\tau}^t b_{k,t,i} \frac{C_a}{\sqrt{k+t_0}} + \gamma \sup_{i \in \mathcal{N}} \sum_{k=\tau}^t b_{k,t,i} \frac{C'_a}{k+t_0} + \frac{C_\epsilon}{\sqrt{t+1+t_0}} + \frac{C_\phi}{t+1+t_0} \\ &\leq \left(\frac{\tau+t_0}{t+1+t_0} \right)^{\sigma h} a_\tau + \frac{C_\phi}{t+1+t_0} + \gamma \sup_{i \in \mathcal{N}} \sum_{k=\tau}^t b_{k,t,i} \frac{C'_a}{k+t_0} + \gamma \sup_{i \in \mathcal{N}} \sum_{k=\tau}^t b_{k,t,i} \frac{C_a}{\sqrt{k+t_0}} + \frac{C_\epsilon}{\sqrt{t+1+t_0}} \end{aligned}$$

where we use the bound for $\tilde{\beta}_{k,t}$ in Lemma 6. To finish the final step of the proof, we need the aid of the following lemma.

Lemma 10 (Adapted from Lemma 15 in [76]). *If $\sigma h(1 - \sqrt{\gamma}) \geq 1$, $t_0 \geq 1$ and $\alpha_0 \leq \frac{1}{2M}$. Then for any $i \in \mathcal{N} = \{1, 2, \dots, n\}$ and any $\omega \in (0, 1]$, we have,*

$$\sum_{k=\tau}^t b_{k,t,i} \frac{1}{(k+t_0)^\omega} \leq \frac{1}{\sqrt{\gamma}(t+1+t_0)^\omega}.$$

Proof. Denote $e_t = \sum_{k=\tau}^t b_{k,t,i} \frac{1}{(k+t_0)^\omega}$. We use induction to show that $e_t \leq \frac{1}{\sqrt{\gamma}(t+1+t_0)^\omega}$. The conclusion is true for $t = \tau$ as $\hat{\alpha}_\tau \leq M\alpha_\tau \leq \frac{1}{2}$, then $e_\tau = b_{\tau,\tau,i} \frac{1}{(\tau+t_0)^\omega} = \hat{\alpha}_\tau d_{\tau,i} \frac{1}{(\tau+t_0)^\omega} \leq \frac{1}{\sqrt{\gamma}(\tau+1+t_0)^\omega}$ due to $\left(1 + \frac{1}{t_0}\right)^\omega \leq 1 + \frac{1}{t_0} \leq 2 \leq \frac{2}{\sqrt{\gamma}}$, $t_0 \geq 1, \omega \leq 1$. Then we assume the statement is true for $t-1$, then we have

$$\begin{aligned} e_t &= \sum_{k=\tau}^{t-1} b_{k,t,i} \frac{1}{(k+t_0)^\omega} + b_{t,t,i} \frac{1}{(t+t_0)^\omega} = (1 - \hat{\alpha}_t d_{t,i}) \sum_{k=\tau}^{t-1} b_{k,t-1,i} \frac{1}{(k+t_0)^\omega} + \hat{\alpha}_t d_{t,i} \frac{1}{(t+t_0)^\omega} \\ &= (1 - \hat{\alpha}_t d_{t,i}) e_{t-1} + \hat{\alpha}_t d_{t,i} \frac{1}{(t+t_0)^\omega} \leq (1 - \hat{\alpha}_t d_{t,i}) \frac{1}{\sqrt{\gamma}(t+t_0)^\omega} + \hat{\alpha}_t d_{t,i} \frac{1}{(t+t_0)^\omega} \\ &= [1 - \hat{\alpha}_t d_{t,i}(1 - \sqrt{\gamma})] \frac{1}{\sqrt{\gamma}(t+t_0)^\omega} \leq [1 - \alpha_t M \sigma (1 - \sqrt{\gamma})] \frac{1}{\sqrt{\gamma}(t+t_0)^\omega} = \left[1 - \frac{h}{t+t_0} \sigma (1 - \sqrt{\gamma}) \right] \frac{1}{\sqrt{\gamma}(t+t_0)^\omega} \\ &= \left[1 - \frac{\sigma h}{t+t_0} (1 - \sqrt{\gamma}) \right] \left(\frac{t+1+t_0}{t+t_0} \right)^\omega \frac{1}{\sqrt{\gamma}(t+1+t_0)^\omega} = \left[1 - \frac{\sigma h}{t+t_0} (1 - \sqrt{\gamma}) \right] \left(1 + \frac{1}{t+t_0} \right)^\omega \frac{1}{\sqrt{\gamma}(t+1+t_0)^\omega}, \end{aligned}$$

where we have used the fact that $\hat{\alpha}_k \geq \alpha_k$ and $d_{t,i} \geq M\sigma$. Using the fact that for any $x > -1$, $(1+x) \leq e^x$, we have,

$$\left[1 - \frac{\sigma h}{t+t_0}(1-\sqrt{\gamma})\right] \left(1 + \frac{1}{t+t_0}\right)^\omega \leq e^{-\frac{\sigma h}{t+t_0}(1-\sqrt{\gamma}) + \omega \frac{1}{t+t_0}} \leq 1,$$

where we have used $\omega \leq 1$ and $\sigma h(1-\sqrt{\gamma}) \geq 1$, therefore $\omega - \sigma h(1-\sqrt{\gamma}) \leq 0$. Thus, we have

$$e_t \leq \left[1 - \frac{\sigma h}{t+t_0}(1-\sqrt{\gamma})\right] \left(1 + \frac{1}{t+t_0}\right)^\omega \frac{1}{\sqrt{\gamma}(t+1+t_0)^\omega} \leq \frac{1}{\sqrt{\gamma}(t+1+t_0)^\omega}.$$

This finishes the induction, and concludes the proof of this lemma. \square

By using Lemma 10 and setting $\omega = 1, \frac{1}{2}$, respectively, we have

$$\begin{aligned} a_{t+1} &\leq \left(\frac{\tau+t_0}{t+1+t_0}\right)^{\sigma h} a_\tau + \frac{C_\phi}{t+1+t_0} + \gamma \sup_{i \in \mathcal{N}} \sum_{k=\tau}^t b_{k,t,i} \frac{C'_a}{k+t_0} + \gamma \sup_{i \in \mathcal{N}} \sum_{k=\tau}^t b_{k,t,i} \frac{C_a}{\sqrt{k+t_0}} + \frac{C_\epsilon}{\sqrt{t+1+t_0}} \\ &\leq \left(\frac{\tau+t_0}{t+1+t_0}\right)^{\sigma h} a_\tau + \frac{C_\phi}{t+1+t_0} + \sqrt{\gamma} \frac{C'_a}{t+1+t_0} + \sqrt{\gamma} \frac{C_a}{\sqrt{t+1+t_0}} + \frac{C_\epsilon}{\sqrt{t+1+t_0}}. \end{aligned}$$

Denote $F_t = \sqrt{\gamma} \frac{C_a}{\sqrt{t+1+t_0}} + \frac{C_\epsilon}{\sqrt{t+1+t_0}}$ and $F'_t = \sqrt{\gamma} \frac{C'_a}{t+1+t_0} + \frac{C_\phi}{t+1+t_0} + \left(\frac{\tau+t_0}{t+1+t_0}\right)^{\sigma h} a_\tau$,

then we have $a_{t+1} \leq F_t + F'_t$. It suffices to show $F_t \leq \frac{C_a}{\sqrt{t+1+t_0}}$, $F'_t \leq \frac{C'_a}{t+1+t_0}$.

Notice that $\frac{C_\epsilon}{C_a} = \frac{6\bar{\epsilon} \sqrt{\frac{(\tau+1)h}{\sigma} \log\left(\frac{2(\tau+1)t^2 n}{\delta}\right)}}{\frac{12\bar{\epsilon}}{1-\gamma} \sqrt{\frac{(\tau+1)h}{\sigma} \log\left(\frac{2(\tau+1)T^2 n}{\delta}\right)}} \leq \frac{1-\gamma}{2} \leq 1 - \sqrt{\gamma}$. The last inequality is a direct result

of the fact that $(\sqrt{\gamma}-1)^2 \geq 0$. Thus $F_t \leq \frac{C_a}{\sqrt{t+1+t_0}}$.

We also notice that $\frac{a_\tau(\tau+t_0)}{C'_a} \leq \frac{2r_{\max} \tau+t_0}{1-\gamma} \frac{1-\gamma}{C'_a} \leq \frac{1-\gamma}{4} \leq \frac{1-\sqrt{\gamma}}{2}$. Furthermore, we have $\frac{C_\phi}{C'_a} \leq \frac{1-\gamma}{4} \leq \frac{1-\sqrt{\gamma}}{2}$. Then, we have

$$\begin{aligned} F'_t &= \sqrt{\gamma} \frac{C'_a}{t+1+t_0} + \frac{C_\phi}{t+1+t_0} + \left(\frac{\tau+t_0}{t+1+t_0}\right)^{\sigma h} a_\tau \leq \sqrt{\gamma} \frac{C'_a}{t+1+t_0} + \frac{C_\phi}{t+1+t_0} + \frac{a_\tau(\tau+t_0)}{t+1+t_0} \\ &\leq \sqrt{\gamma} \frac{C'_a}{t+1+t_0} + \frac{1-\sqrt{\gamma}}{2} \frac{C'_a}{t+1+t_0} + \frac{1-\sqrt{\gamma}}{2} \frac{C'_a}{t+1+t_0} = \frac{C'_a}{t+1+t_0} \end{aligned}$$

This finishes the induction, and we have $a_T \leq \frac{C_a}{\sqrt{T+t_0}} + \frac{C'_a}{T+t_0}$, where $C_a = \frac{12\bar{\epsilon}}{1-\gamma} \sqrt{\frac{(\tau+1)h}{\sigma} \log\left(\frac{2(\tau+1)T^2 n}{\delta}\right)}$,

$C'_a = \frac{4}{1-\gamma} \max(C_\phi, \frac{2(\tau+t_0)r_{\max}}{1-\gamma})$, $C_\phi = \frac{16\bar{\epsilon}h\tau}{\sigma}$. Based on Lemma 5, we have $\bar{\epsilon} := \frac{4r_{\max}}{1-\gamma} + C$ where

$C \leq (1+\gamma)\|x^*\| \leq 2\frac{r_{\max}}{1-\gamma}$. Therefore, we have $\bar{\epsilon} \leq \frac{6r_{\max}}{1-\gamma}$. Taken together with $\tau = \lceil \log_2(\frac{2}{\mu_{\min}}) \rceil t_{\text{mix}}$

and $\sigma = \frac{\mu_{\min}}{2}$, we have with probability at least $1-\delta$,

$$\begin{aligned} \|\hat{Q}_T - Q^*\| &\leq \frac{72r_{\max}}{(1-\gamma)^2} \sqrt{\frac{2(\lceil \log_2(\frac{2}{\mu_{\min}}) \rceil t_{\text{mix}} + 1)h}{\mu_{\min}(T+t_0)} \log\left(\frac{2(\lceil \log_2(\frac{2}{\mu_{\min}}) \rceil t_{\text{mix}} + 1)T^2 |\mathcal{S}| |\mathcal{A}|}{\delta}\right)} \\ &\quad + \frac{4r_{\max}}{(1-\gamma)^2} \max\left(\frac{192h \lceil \log_2(\frac{2}{\mu_{\min}}) \rceil t_{\text{mix}}}{\mu_{\min}}, 2\left(\lceil \log_2(\frac{2}{\mu_{\min}}) \rceil t_{\text{mix}} + t_0\right)\right) \frac{1}{T+t_0} \\ &\simeq \tilde{\mathcal{O}}\left(\frac{r_{\max} \sqrt{t_{\text{mix}}}}{(1-\gamma)^{2.5} \mu_{\min}} \frac{1}{\sqrt{T}} + \frac{r_{\max} t_{\text{mix}}}{(1-\gamma)^3 \mu_{\min}^2} \frac{1}{T}\right). \end{aligned}$$

The above inequality holds when we take $h = \Theta(\frac{1}{\mu_{\min}(1-\gamma)})$, $t_0 = \tilde{\Theta}(\max(\frac{1}{\mu_{\min}(1-\gamma)}, t_{\text{mix}}))$. The whole proof is thus completed. \square

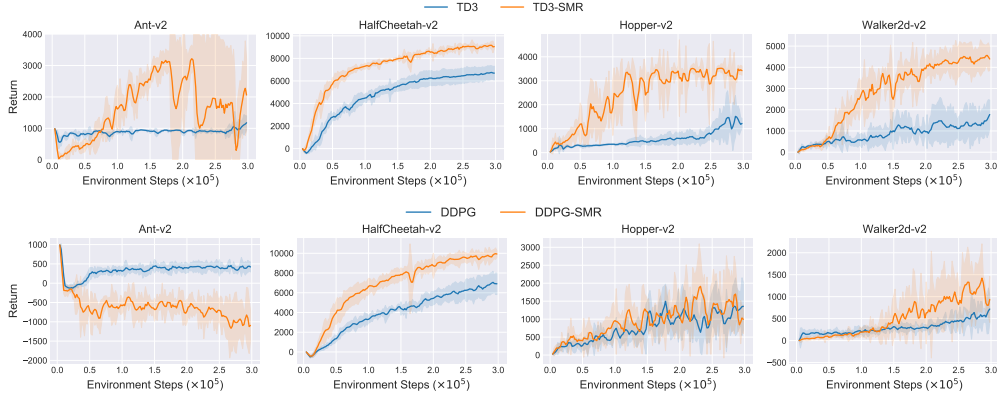


Figure 10: Experimental results of TD3-SMR against TD3 and DDPG-SMR against DDPG. The results are averaged over 6 random seeds, and the shaded region denotes the standard deviation.

B.8 Proof of Corollary 2

Corollary 4 (Sample complexity). *For any $0 < \delta < 1$ and $0 < \epsilon < 1$, with Q -SMR algorithm we have:*

$$\forall (s, a) \in \mathcal{S} \times \mathcal{A} : \|\hat{Q}_T - Q^*\|_\infty \leq \epsilon, \quad (31)$$

holds with probability at least $1 - \delta$, provided the iteration number T obeys:

$$T \gtrsim \frac{r_{\max}^2 t_{\text{mix}}}{(1 - \gamma)^5 \mu_{\min}^2 \epsilon^2}. \quad (32)$$

Proof. The proof is quite straightforward. Since $\|\hat{Q}_T - Q^*\| \leq \tilde{\mathcal{O}} \left(\frac{r_{\max} \sqrt{t_{\text{mix}}}}{(1 - \gamma)^{2.5} \mu_{\min}} \frac{1}{\sqrt{T}} + \frac{r_{\max} t_{\text{mix}}}{(1 - \gamma)^3 \mu_{\min}^2} \frac{1}{T} \right)$. Reaching an accuracy of ϵ means that $\frac{r_{\max} \sqrt{t_{\text{mix}}}}{(1 - \gamma)^{2.5} \mu_{\min}} \frac{1}{\sqrt{T}} + \frac{r_{\max} t_{\text{mix}}}{(1 - \gamma)^3 \mu_{\min}^2} \frac{1}{T} \leq \epsilon$. With the scale of $\frac{1}{\sqrt{T}}$ and $\frac{1}{T}$, $\frac{r_{\max} \sqrt{t_{\text{mix}}}}{(1 - \gamma)^{2.5} \mu_{\min}} \frac{1}{\sqrt{T}} \leq \epsilon$ is sufficient, which leads to $T \geq \frac{r_{\max}^2 t_{\text{mix}}}{(1 - \gamma)^5 \mu_{\min}^2 \epsilon^2}$. \square

C Missing Experimental Results and Details

In this section, we provide some missing experimental results and details. We first demonstrate the experimental results of TD3-SMR and DDPG-SMR, and we also show how reducing SMR ratio and increasing batch size will affect them. We then list the full results of SAC-SMR on DMC suite [91] and PyBullet-Gym [23], including state-based tasks and image-based tasks. Furthermore, we show that SMR can boost the sample efficiency of the base algorithm with longer online interactions (1M online interactions). We also conduct experiments on Arcade Learning Environment (Atari) where we combine SMR with DQN [67]. Finally, we show that SMR can improve sample efficiency regardless of the initial learning rate.

C.1 Performance of TD3-SMR and DDPG-SMR

We summarize the full performance comparison of TD3-SMR against the vanilla TD3 as well as DDPG-SMR versus DDPG (here we use our DDPG from [29]) on four continuous control tasks from OpenAI Gym [8] in Figure 10. We use $M = 10$ by default. We notice that the sample efficiency of both TD3 and DDPG benefit greatly from SMR on many of the evaluated tasks. While we do observe a sort of performance instability on Ant-v2 for TD3-SMR, and find that DDPG-SMR underperforms the vanilla DDPG. For TD3, this may be because the neural networks encounter the phenomenon of overfitting in this environment. While for DDPG, this may be due to the fact that *SMR does not modify the way of value estimation*, indicating that the phenomenon of overestimation still exists in DDPG-SMR. The overestimation bias can be accumulated during the sample reuse loop on Ant-v2, resulting in poor performance. On other tasks, we find that SMR consistently aids the sample efficiency of the base algorithm for both TD3 and DDPG, often by a large margin. As mentioned in Section 6.2, the ways of remedying the overfitting phenomenon can be (1) using smaller M , e.g., $M = 5$; (2) resetting the agent periodically; (3) leveraging a larger batch size; etc. We show below the effectiveness of part of them, including using a smaller SMR ratio and using a larger batch size.

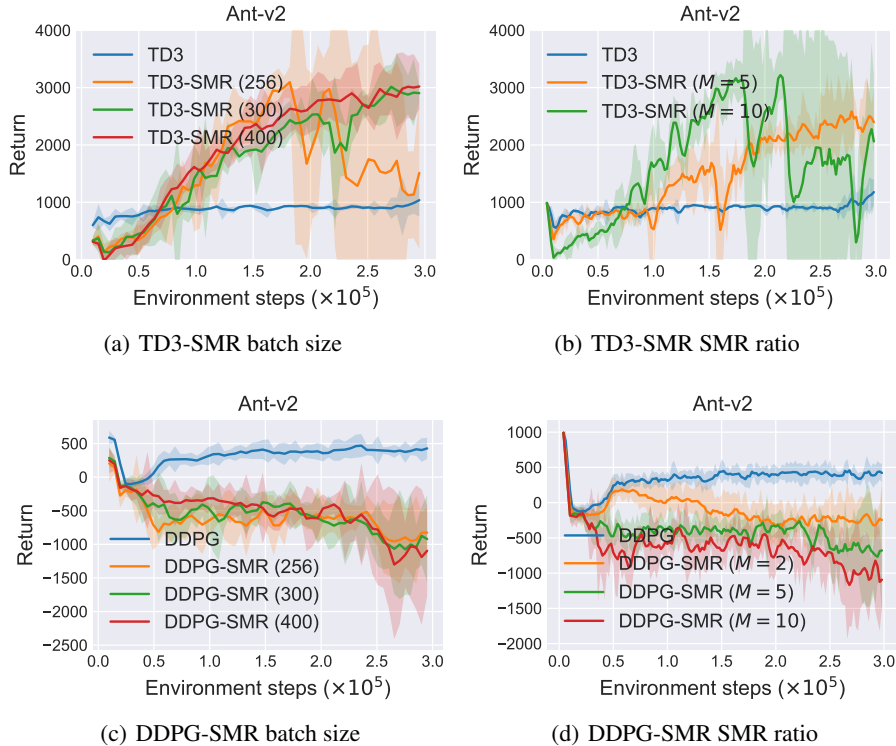


Figure 11: Performance comparison of TD3-SMR and DDPG-SMR against their base algorithms on Ant-v2. (a) TD3-SMR with different batch sizes where we sweep over $\{256, 300, 400\}$; (b) TD3-SMR with different SMR ratios M where we compare TD3-SMR ($M = 10$) against TD3-SMR ($M = 5$); (c) DDPG-SMR with different batch sizes in $\{256, 300, 400\}$; (d) DDPG-SMR with different SMR ratios M , $M \in \{2, 5, 10\}$. We report the mean performance along with the standard deviation over 6 different random seeds.

We summarize the empirical results in Figure 11, where we run for 300K online interactions and evaluate the agent every 1000 timesteps over 10 trials. We find that using a smaller SMR ratio or using a larger batch size is beneficial to the stability and satisfying performance for TD3-SMR as shown in Figure 11(a) and 11(b). However, it can be seen that DDPG-SMR does not seem to benefit from either a smaller SMR ratio M (even $M = 2$) or a larger batch size. Using a smaller SMR ratio or larger batch size can help improve DDPG-SMR with $M = 10$ to some extent. While they still underperform vanilla DDPG. This is due to *SMR only enforces more updates on the fixed batch data instead of dealing with overestimation bias*. As shown in Equation 9, SMR tends to *smooth the gradient for updating* by leveraging the gradient of intermediate values. On tasks like HalfCheetah-v2 and Walker2d-v2, SMR can benefit DDPG by better exploiting collected data, while on some tasks like Ant-v2, DDPG-SMR does not seem to be able to escape from the curse of overestimation bias. We, therefore, recommend the application of SMR upon off-policy continuous control algorithms that can address the overestimation bias themselves, e.g., TD3 [29] by using clipped double Q-learning; TQC [50] by truncating small proportion of estimated Q distribution, etc.

C.2 Omitted results from DMC suite and PyBullet-Gym

We demonstrate in this subsection the missing experimental results of SAC-SMR on DMC suite [91] and PyBullet-Gym [23]. The performance comparison of SAC-SMR and SAC is available in Figure 12. As expected, we observe that SAC-SMR outperforms the vanilla SAC on all of the evaluated state-based tasks. These further show that SMR can benefit the sample efficiency of the base algorithm on a wide range of different tasks.

We further demonstrate in Figure 13 the experimental results on 4 additional image-based tasks from DMC suite. Note that we run experiments on DMC suite 100K benchmarks for SAC-SMR. For image-based tasks, we use a comparatively small SMR ratio $M = 5$ as it will be very time-consuming to adopt a $M = 10$ (image-based tasks already take much longer time to run than state-based tasks). For example, it takes about 4 hours to run with SAC on *reacher-easy* while it takes about 15 hours to run with SAC-SMR ($M = 5$) on this task. If we

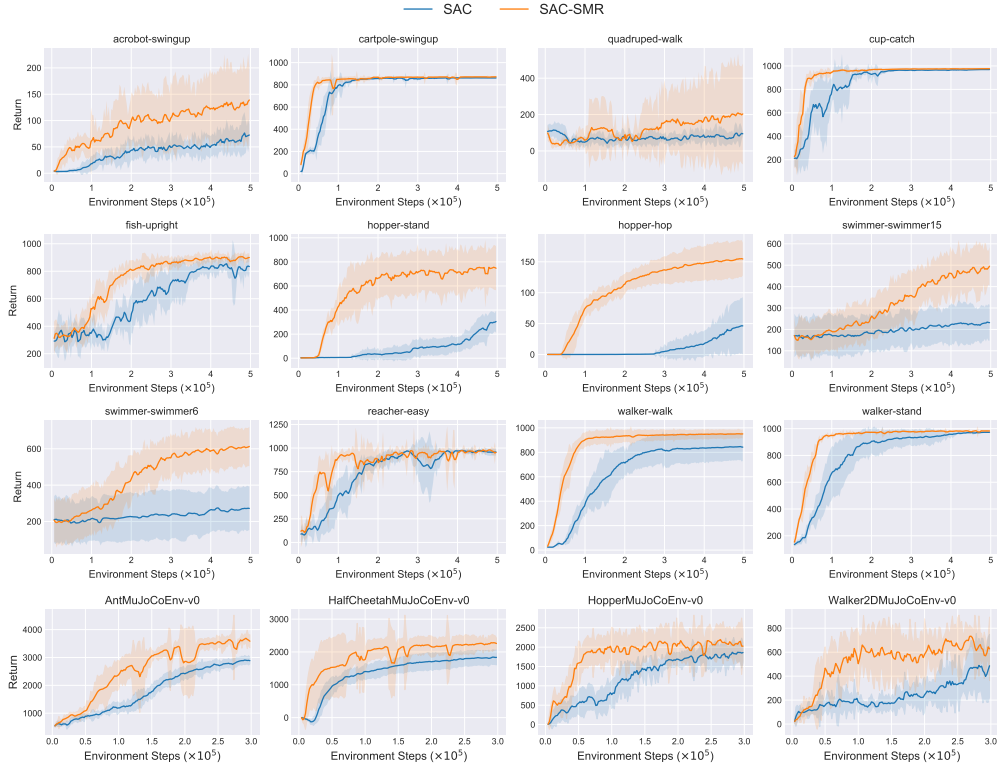


Figure 12: Experimental results of SAC-SMR against SAC on state-based tasks from DMC suite and PyBullet-Gym. The results are averaged over 6 random seeds with 500K online interactions, and the shaded region denotes the standard deviation.

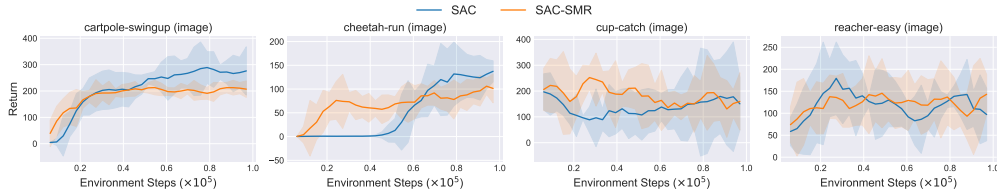


Figure 13: Experimental results on 4 image-based tasks from DMC suite 100K benchmarks. The results are averaged over 6 different random seeds, and the shaded region denotes the standard deviation.

adopt $M = 10$, it will take more than 24 hours. We observe that on some of the image-based tasks, our SMR can boost the sample efficiency of SAC, e.g., SAC-SMR learns faster than vanilla SAC on `cheetah-run` and beats SAC on `cup-catch`. While we also see that SAC-SMR kind of underperforming SAC on `cartpole-swingup` and `reacher-easy`. In fact, we do not see a large margin on image-based tasks as on the state-based tasks. We attribute the reason to *bad representation*. We usually leverage an encoder to deal with image input, where we do representation learning to reduce the size of the input. However, the parameters of the encoder are also continually updated during the training process. The error in representations accumulates and may impede the agent from learning better policy. For some of the tasks, SMR can benefit the agent, while on some tasks, things are different. SMR can benefit the state-based tasks as the states are *precise representation* of the information that the agent needs to perform control. This phenomenon also exists on Atari tasks, one can refer to Appendix C.4 for more details. Furthermore, as mentioned in [103], the automatic entropy adjustment strategy in SAC is inadequate and in some cases may result in a premature *entropy collapse*. This will in turn prevent the agent from finding more optimal behaviors. SMR can somewhat worsen this phenomenon due to multiple updates on the sampled batch. These we believe can explain the failure of SAC-SMR on some of the image-based tasks.

One interesting question is: whether more advanced methods for image-based tasks can benefit from SMR? To answer this question, we select the most recent DrQ-v2 [103] and combine it with our SMR. DrQ-v2 is built upon

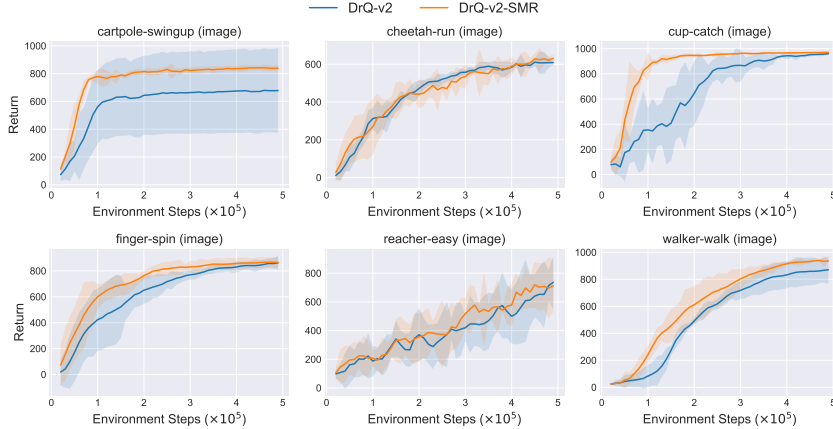


Figure 14: Experimental results of DrQ-v2-SMR against vanilla DrQ-v2 on six image-based tasks from DMC suite. Each algorithm is run for 500K frames and evaluated over 10 trials every 1000 frames. The results are averaged over 6 different random seeds. We report the mean performance and the standard deviation.

Table 3: Performance comparison of DrQ-v2 and DrQ-v2-SMR on six image-based tasks from DMC suite. The numbers indicate the performance achieved when the specific number of frames is seen. We **bold** the best mean results.

Tasks	DrQ-v2	DrQ-v2-SMR
cartpole-swingup@500K	682.7±304.8	842.5±25.2
cheetah-run@500K	605.5±12.3	626.5±17.8
cup-catch@500K	965.6±5.9	970.2±5.1
finger-spin@500K	867.7±55.0	872.0±39.3
reacher-easy@500K	736.8±185.5	736.2±182.1
walker-walk@500K	869.5±102.6	949.3±8.9

DrQ [104], an actor-critic approach that uses data augmentation to learn directly from pixels. The improvements of DrQ-v2 over DrQ include: (1) switch SAC to DDPG (to avoid entropy collapse); (2) incorporate n -step returns to estimate temporal difference (TD); (3) introduce a decaying schedule for exploration noise error; (4) improve running speed; (5) find better hyperparameters. We adopt the SMR ratio $M = 5$ as we do for image-based tasks in SAC-SMR. We demonstrate in Figure 14 that DrQ-v2-SMR can outperform DrQ-v2 on most of the evaluated tasks (e.g., `cup-catch`, `cartpole-swingup`) and is competitive to DrQ-v2 on other tasks (e.g., `cheetah-run`). We also compare the final performance of DrQ-v2 and DrQ-v2-SMR at 500K frames in Table 3, where we unsurprisingly find the advantage of DrQ-v2-SMR over DrQ-v2. The success of SMR upon DrQ-v2 may due to (1) no entropy collapse and better exploration mechanism; (2) data augmentation to help alleviate the negative influence of initial bad representation.

Note that DrQ-v2-SMR spends 3 times of training time than DrQ-v2. Thanks to the fast running speed of DrQ-v2, this cost is comparatively tolerable. For example, DrQ-v2 requires 7 hours on `finger-spin` while DrQ-v2-SMR takes 20 hours.

C.3 Can SMR still work with longer online interactions?

In the main text and the appendix above, we run most of the experiments with only 300K online interactions or 500K online interactions (100K for SAC-SMR on image-based tasks from the DMC suite). Though 300K or 500K (or even fewer) online interactions are widely adopted for examining sample efficiency in model-based methods [44, 71, 51, 101] and REDQ [11], one may wonder whether our method can consistently improve sample efficiency with longer online interactions. To address this concern, we run SAC-SMR ($M = 10$) on 16 tasks from the DMC suite for a typical 1M online interactions. Each algorithm is evaluated every 1000 timesteps over 10 trials. We summarize the empirical results in Figure 15 where SAC-SMR significantly outperforms vanilla SAC on all of the evaluated tasks by a remarkable margin. SAC-SMR can converge faster and learn faster with longer online interactions.

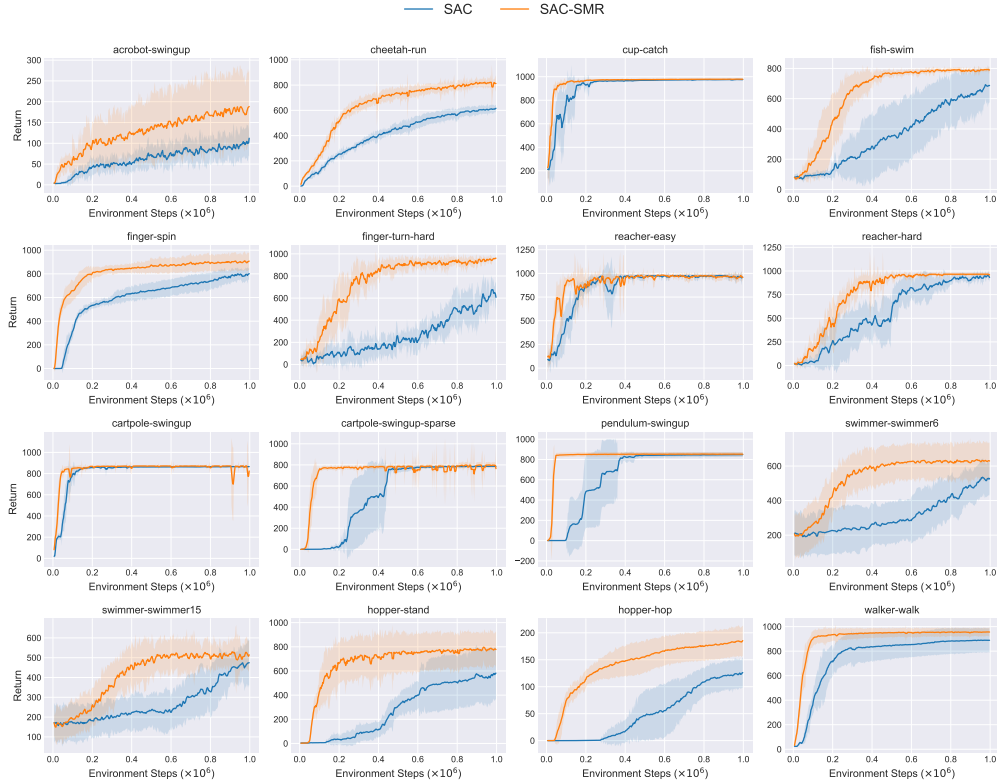


Figure 15: Experimental results of SAC-SMR against SAC on 16 tasks from DMC suite. All methods are run for 1M online interactions, The results are averaged over 6 different random seeds and the shaded region represents the standard deviation.

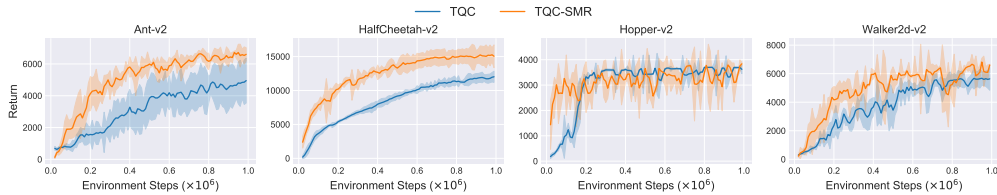


Figure 16: Experimental results of TQC-SMR against TQC on 4 tasks from OpenAI Gym. All methods are run for 1M online interactions, The results are averaged over 6 different random seeds and the shaded region represents the standard deviation.

Furthermore, we run TQC-SMR and TQC for 1M online interactions on 4 OpenAI Gym environments to show the generality of the above conclusion. We summarize the empirical results in Figure 16. It can be seen that SMR consistently improves the sample efficiency of TQC with longer interactions, often surpassing the base algorithm by a large margin. We believe the evidence above are enough to show that SMR does aid sample efficiency with longer interactions.

The concern on whether SMR aids sample efficiency with longer interactions is strongly correlated with the concern on the asymptotic performance of SMR. One can find in Figure 15 and 16 that the asymptotic performance of SMR upon different baseline algorithms are actually quite good. For example, on many tasks like *finger-turn-hard*, *reacher-hard*, SAC-SMR converges very fast and achieves the highest possible return on them. Meanwhile, as we emphasize in the main text, we do not mean that the users have to always use a large SMR ratio if one worries about overfitting. SMR can serve as a quite good warm-up strategy, i.e., utilizing SMR (with SMR ratio $M = 10$) for some initial interactions (e.g., 300K) and then resume vanilla training process (with SMR ratio $M = 1$). In this way, one can enjoy both good sample efficiency from SMR and good asymptotic performance from the vanilla algorithm.

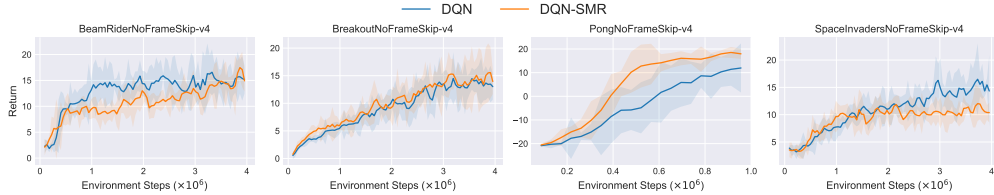


Figure 18: Empirical results of DQN-SMR against DQN on four tasks from Atari. The results are averaged over 5 different random seeds with the shaded region denoting standard deviation.

C.4 Experimental results on Atari

We show in the main text that Q-SMR significantly outperforms Q-learning on two discrete control tasks. One may naturally ask: can SMR aid the sample efficiency of DQN on Arcade Learning Environment [5]? To answer this question, we conduct experiments on one typical environment `PongNoFrameSkip-v4`. We adopt the original way of processing the Atari image input, i.e., map the image ($3 \times 84 \times 84$) into an embedding of size $32 \times 7 \times 7$ with convolutional networks. Then, this representation is passed into an MLP with a hidden layer size of 256 to get Q -value estimate. We keep the default hyperparameters of DQN unchanged and only incorporate a sample reuse loop in it to yield DQN-SMR. It can be found in Figure 17 that DQN-SMR with SMR ratio $M = 10$ remarkably outperforms DQN on Pong. However, It takes about **84 hours** for DQN-SMR to run 500K frames on Pong, which is 8.7 times slower than DQN (9.6 hours). The computation cost is due to the fact that the size of image input is very large, and it takes time for the network to process it. Updating on the fixed batch (which SMR does) will inevitably worsen the situation and take longer time to train the agent. Considering that there are many advanced methods for discrete control with image input like EfficientZero [105] (which solves Atari within 2 hours of real-time game play), MuZero [79], Dreamer v2 [34], SimPLe [45], it is **STRONGLY NOT RECOMMENDED** to adopt SMR on image-based tasks like Atari.

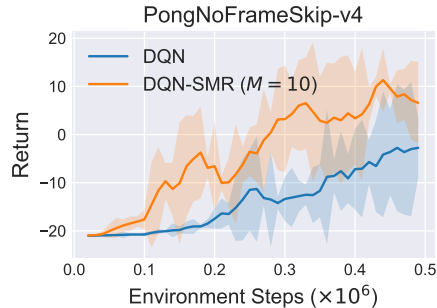


Figure 17: Experimental results of DQN-SMR ($M = 10$) against DQN on `PongNoFrameSkip-v4` task. Each method is run for 500K frames. The results are averaged over 5 random seeds, and the shaded region captures the standard deviation.

However, to show that our method can also work in discrete control settings, we conduct experiments on four environments from Atari. To save training time, we only adopt a small SMR ratio $M = 2$. We run `PongNoFrameSkip-v4` for 1M frames, and other tasks for 4M frames. Each algorithm is evaluated every 5000 timesteps over 10 trials. The results are summarized in Figure 18.

It is interesting to see that DQN-SMR outperforms DQN on `PongNoFrameSkip-v4` and is slightly better than DQN on `BreakoutNoFrameSkip-v4`. However, DQN-SMR underperforms DQN on `BeamRiderNoFrameSkip-v4` and only exceeds DQN at the last few online interactions. DQN-SMR learns faster than DQN at first several timesteps on `SpaceInvadersNoFrameSkip-v4` and underperforms DQN afterwards. Such a phenomenon is due to the fact that the encoder in the DQN network (convolutional layers) is also continually updated during training. At the first several steps, the encoder may output bad representations for the task, indicating that the resulting representations are actually biased and inaccurate. With the sample reuse loop on these bad representations, it will become harder for the network to learn the correct knowledge and policy for this control task. For some of the tasks, the agent may successfully get rid of this dilemma, while on some other tasks, the agent may get stuck and cannot escape from it. Also, DQN is known to incur overestimation bias [94, 77], which is similar to DDPG. We observe DDPG-SMR underperforms DDPG on `Ant-v2` in Appendix C.1, and the situation is similar here. Meanwhile, though we adopt a very small SMR ratio $M = 2$, it still takes about 2 times longer training time than vanilla DQN, e.g., it takes 18 hours for DQN to run 1M steps on `PongNoFrameSkip-v4`, while it takes 37 hours of training time for DQN-SMR with $M = 2$; it takes 3 days for DQN to run 4M frames on `BreakoutNoFrameSkip-v4`, while it takes about 6 days of training time for DQN-SMR with SMR ratio $M = 2$. We thus do not recommend using SMR loop on image-based tasks. Since we set our focus on the continuous control domain, we do not actively conduct extensive experiments on DQN and its variants (e.g. C51 [4], Rainbow [40]) in discrete control tasks.

C.5 Can SMR benefit base algorithm with different learning rate?

In the main text, we combine SMR with the base algorithm without tuning the hyperparameters. Considering the difference between magnifying learning rate and SMR loop, one may wonder whether SMR can boost the sample efficiency of the base algorithm with different initial learning rates. We answer this by comparing SAC-SMR ($M = 10$) against SAC and conducting experiments on two typical environments from OpenAI Gym [8], HalfCheetah-v2 and Walker2d-v2, under different initial learning rates for actor and critic networks. We sweep the learning rate over $\{1 \times 10^{-3}, 1 \times 10^{-4}, 3 \times 10^{-4}, 3 \times 10^{-5}\}$ (SAC uses a learning rate of 3×10^{-4} by default, one can check the detailed hyperparameter setup for SAC in Appendix D.2). We summarize the empirical results in Figure 19. It is easy to find that SMR notably improves the sample efficiency of SAC upon different initial learning rates, even with a large learning rate 1×10^{-3} . We believe this evidence can alleviate the concern, and validate the effectiveness and generality of SMR.

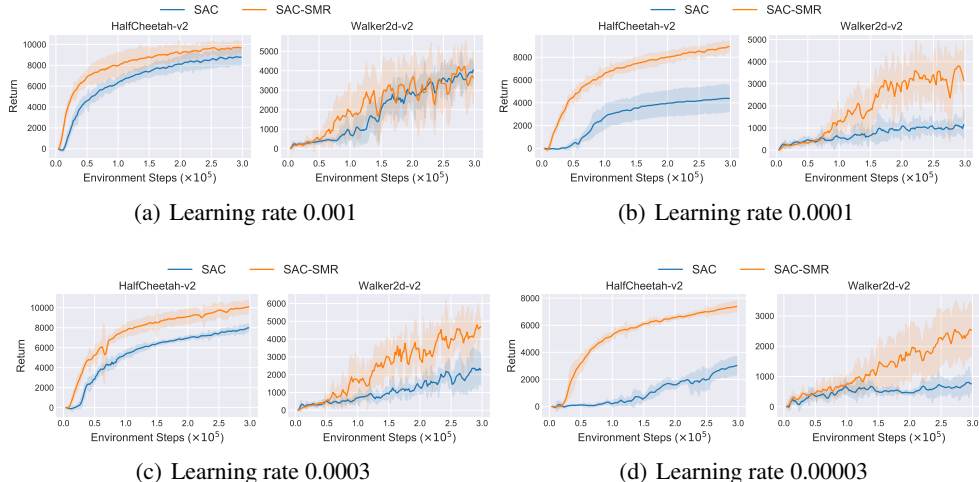


Figure 19: Performance comparison of SAC-SMR with SMR ratio $M = 10$ and SAC on HalfCheetah-v2 and Walker2d-v2 under different initial (fixed) learning rates for actor and critic networks. We sweep the initial learning rate across $\{0.001, 0.0001, 0.0003, 0.00003\}$. The results are averaged over 6 different random seeds and the shaded region denotes the standard deviation.

D Pseudo Codes and Hyperparameters of Off-Policy Algorithms with SMR

In this section, we list the missing details on pseudo codes and hyperparameter setup for off-policy algorithms we adopt in this paper. We first introduce the hyperparameters for Q-learning and Q-SMR (the pseudo codes are omitted, please check Algorithm 1). As we only present the general framework of SMR upon actor-critic architecture in Algorithm 2, we further offer the detailed pseudo codes and hyperparameter setup for various continuous control algorithms.

D.1 Q-learning and Q-SMR

We conduct experiments using Q-SMR and Q-learning on two discrete control tasks, CliffWalking-v0 from OpenAI Gym [8] and maze-random-20x20-plus-v0 from Gym-Maze (please refer to Gym documentation (<https://gymnasium.farama.org/>) and <https://github.com/MattChanTK/gym-maze>). CliffWalking-v0 is a gridworld learning task adapted from Example 6.6 from [87]. It contains 4×12 grids. The agent starts at the bottom-left and aims at reaching the bottom-right. There exists a cliff in the bottom-center, and the agent will return to the start position if it steps on the cliff. The agent can take four actions (move up, move down, move left, and move right). Each episode of game play contains 100 steps. The episode ends if the agent steps on the cliff. We run Q-SMR and Q-learning for 500 episodes and average their performance over 20 independent runs.

maze-random-20x20-plus-v0 is a 2D maze environment where the agent is targeted to find its way from the top left corner to the goal at the bottom right corner. The objective is to find the shortest path from the start to the goal. The agent can also take four actions (move up, move down, move left, and move right) and the observation space is given by the coordinates of the agent. The agent receives a reward of 1 if it reaches the goal position. For every step in the maze, the agent receives an additional reward of $-\frac{0.1}{\#cells}$, where $\#cells$ denotes the number of cells. For maze-random-20x20-plus-v0, there are 20×20 cells. Specially, the agent

Algorithm 3 TD3-SMR

```
1: Initialize critic networks  $Q_{\theta_1}, Q_{\theta_2}$  and actor network  $\pi_\phi$  with random parameters
2: Initialize target networks  $\theta'_1 \leftarrow \theta_1, \theta'_2 \leftarrow \theta_2, \phi' \leftarrow \phi$  and replay buffer  $\mathcal{B} = \{\}$ 
3: for  $t = 1$  to  $T$  do
4:   Select action  $a$  with exploration noise  $a \sim \pi_\phi(s) + \epsilon$ , where  $\epsilon \sim \mathcal{N}(0, \sigma)$  and observe reward  $r$ , new state  $s'$ 
5:   Store transitions in the replay buffer, i.e.,  $\mathcal{B} \leftarrow \mathcal{B} \cup \{(s, a, r, s')\}$ 
6:   Sample  $N$  transitions  $\{(s_j, a_j, r_j, s'_j)\}_{j=1}^N \sim \mathcal{B}$ 
7:   for  $m = 1$  to  $M$  do
8:      $\tilde{a} \sim \pi_{\phi'}(s') + \epsilon, \epsilon \sim \text{clip}(\mathcal{N}(0, \bar{\sigma}), -c, c)$ 
9:      $y \leftarrow r + \gamma \min_{i=1,2} Q_{\theta'_i}(s', \tilde{a})$ 
10:    Update critic  $\theta_i$  by minimizing  $\frac{1}{N} \sum_s (Q_{\theta_i}(s, a) - y)^2$ 
11:    if  $t \bmod d$  then
12:      Update actor  $\phi$  by deterministic policy gradient  $\nabla_\phi J(\phi) = \frac{1}{N} \sum_s \nabla_a Q_{\theta_1}(s, a)|_{a=\pi_\phi(s)} \nabla_\phi \pi_\phi(s)$ 
13:      Update target networks:  $\theta'_i \leftarrow \tau \theta_i + (1 - \tau) \theta'_i, \phi' \leftarrow \tau \phi + (1 - \tau) \phi'$ 
14:    end if
15:  end for
16: end for
```

can *teleport* from a portal to another portal of the same color. We run Q-SMR and Q-learning for 100 episodes where each episode contains 40000 steps. The maze will be reset if the episode terminates.

For both two environments, we use a learning rate of $\alpha = 0.05$, discount factor $\gamma = 0.99$, and exploration rate $\epsilon = 0.1$ (ϵ -greedy) for the training process. Unlike DQN, we use a fixed exploration rate and learning rate instead of decaying them. During the evaluation, we use an exploration rate of $\epsilon = 0$. We adopt random seeds of 0-19 for simplicity.

D.2 Continuous control algorithms

In our experiments, we use MuJoCo 2.0 with Gym version 0.18.3 and PyTorch [73] version 1.8. We conduct experiments on MuJoCo “-v2” environments and PyBullet “-MuJoCoEnv-v0” environments.

We present in Algorithm 3 the pseudo code for TD3-SMR. We omit the pseudo code for SAC-SMR since it is much similar to that of TD3-SMR. Compared to the original TD3, TD3-SMR only injects a sample reuse loop (see line 7-15 of Algorithm 3), which is the only modification. We list in Table 4 the hyperparameters for SAC, TD3, and SAC-SMR, TD3-SMR where SAC-SMR and TD3-SMR share identical parameters with their base algorithms. We keep the hyperparameters of all these algorithms fixed on all of the evaluated tasks. Our parameter setup generally resembles [31, 30]. It is worth noting that this hyperparameter setup is slightly different from the original TD3, where network size (400, 300), learning rate 1×10^{-3} and batch size 100 are adopted (see [29]). As the authors mentioned (please see <https://github.com/sfujim/TD3>), the parameter setup for TD3 is now different from the original paper. We therefore choose to follow the current hyperparameter setup in the authors’ official implementation.

We list the pseudo code for DARC-SMR [64] in Algorithm 4 and its hyperparameter setup in Table 4. We follow the original hyperparameter setup of the DARC paper and adopt the network size (400, 300) for both the actor network and critic network. For the weighting coefficient ν in DARC (for balancing the underestimation bias and overestimation bias), we also follow the best recommended hyperparameter by the authors, where we adopt $\nu = 0.15$ for Hopper-v2, $\nu = 0.25$ for Ant-v2, and $\nu = 0.1$ for HalfCheetah-v2 and Walker2d-v2. For the regularization parameter λ in DARC, we use $\lambda = 0.005$ by default. Other parameters are identical to the original paper and we keep them unchanged throughout our experiments. We use the official implementation of DARC (<https://github.com/dmksjff/DARC>) when conducting experiments.

We further combine SMR with TQC [50] and list the pseudo code for TQC-SMR in Algorithm 5, with its hyperparameter setup listed in Table 4. Similarly, we follow the default hyperparameter recommended by the authors, e.g., the actor network has a network size of (256, 256), while the critic network has a size of (512, 512, 512). The agent starts training when 256 samples are collected. For the most critical hyperparameter, the number of dropped atoms d , we follow the original paper and adopt $d = 5$ for Hopper-v2, $d = 0$ for HalfCheetah-v2, and $d = 2$ for Ant-v2 and Walker2d-v2. For TD3-SMR, SAC-SMR, and TQC-SMR, we adopt an SMR ratio $M = 10$ by default for all of the evaluated state-based tasks. We use the official implementation of TQC (https://github.com/SamsungLabs/tqc_pytorch) for all of the experimental evaluation.

Table 4: Hyperparameters setup for TD3 [29], SAC [31], DARC [64], TQC [50], and REDQ [11] on continuous control benchmarks.

Hyperparameter	Value
Shared	
Actor network	(400, 300) for DARC and (256, 256) for others
Batch size	256
Learning rate	1×10^{-3} for DARC and 3×10^{-4} for others
Optimizer	Adam [47]
Discount factor	0.99
Replay buffer size	10^6
Warmup steps	256 for TQC and 5×10^3 for others
Nonlinearity	ReLU
Target update rate	5×10^{-3}
TD3	
Target update interval	2
Critic network	(256, 256)
Exploration noise	$\mathcal{N}(0, 0.1)$
Target noise	0.2
Noise clip	0.5
DARC	
Regularization parameter λ	0.005
Critic network	(400, 300)
SAC	
Critic network	(256, 256)
Target update interval	1
Reward scale	1
Entropy target	$-\dim(\mathcal{A})$
Entropy auto-tuning	True
Maximum log std	2
Minimum log std	-20
TQC	
Critic network	(512, 512, 512)
Number of critic networks	5
Number of atoms	25
Huber loss parameter	1
REDQ	
Critic network	(256, 256)
Update-to-data (UTD) ratio	20
Number of critic networks	10
In-target minimization parameter	2

Algorithm 4 DARC-SMR

- 1: Initialize critic networks $Q_{\theta_1}, Q_{\theta_2}$ and actor networks $\pi_{\phi_1}, \pi_{\phi_2}$ with random parameters
- 2: Initialize target networks $\theta'_1 \leftarrow \theta_1, \theta'_2 \leftarrow \theta_2, \phi'_1 \leftarrow \phi_1, \phi'_2 \leftarrow \phi_2$ and replay buffer $\mathcal{B} = \{\}$
- 3: **for** $t = 1$ to T **do**
- 4: Select action a with $\max_i \max_j Q_{\theta_i}(s, \pi_{\phi_j}(s))$ added $\epsilon \sim \mathcal{N}(0, \sigma)$
- 5: Execute action a and observe reward r , new state s' and done flag d
- 6: Store transitions in the replay buffer, i.e., $\mathcal{B} \leftarrow \mathcal{B} \cup \{(s, a, r, s', d)\}$
- 7: **for** $i = 1, 2$ **do**
- 8: Sample N transitions $\{(s_j, a_j, r_j, s'_j, d_j)\}_{j=1}^N \sim \mathcal{B}$
- 9: **for** $m = 1$ to M **do**
- 10: Get actions: $a_1 \leftarrow \pi_{\phi'_1}(s') + \epsilon, a_2 \leftarrow \pi_{\phi'_2}(s') + \epsilon, \epsilon \sim \text{clip}(\mathcal{N}(0, \bar{\sigma}), -c, c)$
- 11: Calculate $\hat{V}(s') = (1 - \nu) \max_{k=1,2} \min_{j=1,2} Q_{\theta'_j}(s', a_k) + \nu \min_{k=1,2} \min_{j=1,2} Q_{\theta'_j}(s', a_k),$
- 12: $y \leftarrow r + \gamma(1 - d)\hat{V}(s')$
- 13: Update critic θ_i by minimizing $\frac{1}{N} \sum_s \{(Q_{\theta_i}(s, a) - y)^2 + \lambda [Q_{\theta_1}(s, a) - Q_{\theta_2}(s, a)]^2\}$
- 14: Update actor ϕ_i by maximizing $\frac{1}{N} \sum_s \nabla_a Q_{\theta_i}(s, a)|_{a=\pi_{\phi_i}(s)} \nabla_{\phi_i} \pi_{\phi_i}(s)$
- 15: Update target networks: $\theta'_i \leftarrow \tau \theta_i + (1 - \tau)\theta'_i, \phi'_i \leftarrow \tau \phi_i + (1 - \tau)\phi'_i$
- 16: **end for**
- 17: **end for**
- 18: **end for**

Algorithm 5 TQC-SMR

- 1: Initialize critic networks $Z_{\theta_n}, n \in \{1, 2, \dots, N\}$ and actor network π_{ϕ} with random parameters
- 2: Initialize target networks $\theta'_n \leftarrow \theta_n, n \in \{1, 2, \dots, N\}$ and replay buffer $\mathcal{D} = \{\}$
- 3: Set target entropy $\mathcal{H}_T = -\dim(\mathcal{A}), \alpha = 1$, number of quantiles L , left atom proportion k
- 4: **for** $t = 1$ to T **do**
- 5: Execute action $a \sim \pi_{\phi}$ and observe reward r , new state s'
- 6: Store transitions in the replay buffer, i.e., $\mathcal{D} \leftarrow \mathcal{D} \cup \{(s, a, r, s')\}$
- 7: Sample a mini-batch transitions $B = \{(s, a, r, s')\} \sim \mathcal{D}$
- 8: **for** $m = 1$ to M **do**
- 9: Update temperature parameter via $\nabla_{\alpha} J(\alpha) = \nabla_{\alpha} \mathbb{E}_{B, \pi_{\phi}} [\log \alpha \cdot (-\log \pi_{\phi}(a|s) - \mathcal{H}_T)]$
- 10: Update actor parameter ϕ via $\nabla_{\phi} \mathbb{E}_{B, \pi_{\phi}} \left[\alpha \log \pi_{\phi}(a|s) - \frac{1}{NL} \sum_{l,n=1}^{N,L} \psi_{\theta_n}^l(s, a) \right]$
 // $\psi_{\theta_n}^l, l \in [1, L]$ is the atom at location l
- 11: $y_i = r + \gamma[z_{(i)}(s', a') - \alpha \log \pi_{\phi}(a'|s')]$ // $z_{(i)}$ is the sorted atoms in ascending order,
 $i \in [NL]$
- 12: Update critic parameter θ_n by $\nabla_{\theta_n} \mathbb{E}_{B, \pi_{\phi}} \left[\frac{1}{kNL} \sum_{l=1}^L \sum_{i=1}^{kN} \rho_{\tau_l}(y_i - \psi_{\theta_n}^l) \right]$
 // ρ_{τ_l} is the Huber quantile loss with parameter 1
- 13: Update target networks: $\theta'_n \leftarrow \beta \theta_n + (1 - \beta)\theta'_n, n \in \{1, 2, \dots, N\}$
- 14: **end for**
- 15: **end for**

For REDQ [11], we also keep the original hyperparameters unchanged when combining it with SMR, i.e., it uses a learning rate of 3×10^{-4} and a network size of (256, 256) for both the actor network and critic network, an ensemble size of 10 for critics. REDQ also adopts a high update-to-data (UTD) ratio of $G = 20$ and samples 2 different indices from 10 critics when calculating the target Q value. We summarize the pseudo code for REDQ-SMR in Algorithm 6 and the hyperparameter setup in Table 4. Inspired by the fact that model-based methods often attain higher sample efficiency by using a high UTD ratio (the number of updates taken by the agent compared to the number of actual interactions with the environment), REDQ explores the feasibility of high UTD ratio without a dynamics model on continuous control tasks. As discussed in the main text (Section 7), SMR is different from adopting a high UTD ratio. REDQ and model-based methods update the agent multiple times with bootstrapping, i.e., each time the agent sees different samples and updates on these

Algorithm 6 REDQ-SMR

```

1: Initialize critic networks  $Q_{\theta_i}, i = 1, 2, \dots, N$  and actor network  $\pi_\phi$  with random parameters
2: Initialize target networks  $\theta'_i \leftarrow \theta_i, i = 1, 2, \dots, N$  and replay buffer  $\mathcal{D} = \{\}$ 
3: for  $t = 1$  to  $T$  do
4:   Take one action  $a_t \sim \pi_\phi(\cdot|s_t)$  and observe reward  $r_t$ , new state  $s'_{t+1}$ 
5:   Store transitions in the replay buffer, i.e.,  $\mathcal{D} \leftarrow \mathcal{D} \cup \{(s_t, a_t, r_t, s'_{t+1})\}$ 
6:   for  $g = 1$  to  $G$  do
7:     Sample a mini-batch  $B = \{(s, a, r, s')\} \sim \mathcal{D}$ 
8:     for  $m = 1$  to  $M$  do
9:       Sample a set  $\mathcal{K}$  of  $K$  indices from  $\{1, 2, \dots, N\}$ 
10:      Compute the  $Q$  target  $y = r + \gamma (\min_{i \in \mathcal{K}} Q_{\theta'_i}(s', \tilde{a}') - \alpha \log \pi_\phi(\tilde{a}'|s'))$ ,  $\tilde{a}' \sim \pi_\phi(\cdot|s')$ 
11:      for  $i = 1, 2, \dots, N$  do
12:        Update  $\theta_i$  with gradient descent using  $\nabla_{\theta_i} \frac{1}{|B|} \sum_{(s,a,r,s') \sim B} (Q_{\theta_i}(s, a) - y)^2$ 
13:        Update target networks:  $\theta'_i \leftarrow \tau \theta_i + (1 - \tau) \theta'_i$ 
14:      end for
15:      if  $g = G$  then
16:        Update actor  $\phi$  with gradient ascent using  $\nabla_{\phi} \frac{1}{|B|} \sum_{s \in B} \left( \frac{1}{N} \sum_{j=1}^N Q_{\theta_j}(s, \tilde{a}) - \alpha \log \pi_\phi(\tilde{a}|s) \right)$ ,  $\tilde{a} \sim \pi_\phi(\cdot|s)$ 
17:      end if
18:    end for
19:  end for
20: end for

```

different data multiple times. SMR, however, updates multiple times on the *fixed* batch data for multiple times. Since REDQ already leverages a high UTD ratio, we use an SMR ratio $M = 5$ for REDQ-SMR. It is worth noting that our reported performance of REDQ is slightly different from the original paper. We have tried our best to reproduce the performance of REDQ on MuJoCo tasks. However, as the authors commented in <https://github.com/watchernyu/REDQ>, the performance of REDQ seems to be quite different with different PyTorch [73] version and the reasons are not entirely clear. We thus choose to run REDQ with its official implementation (<https://github.com/watchernyu/REDQ>) and PyTorch 1.8 and report the resulting learning curves.

For image-based tasks, we adopt the environment wrapper from TD-MPC [36] for SAC and SAC-SMR. The image is processed with a 4-layer CNN with kernel size (7, 5, 3, 3), stride (2, 2, 2, 2) and 32 filters per layer. Then the representation is input into a 2-layer MLP with 512 hidden units. We map the raw image input into an embedding of size 200 and repeat the actions every two frames for six evaluated tasks. For DrQ-v2, we use its official implementation (<https://github.com/facebookresearch/drqv2>) and keep its default hyperparameters setup fixed. For DQN experiments on Atari, we adopt the widely used RL playground implementation for DQN (<https://github.com/TianhongDai/reinforcement-learning-algorithms>).

E Compute Infrastructure

In Table 5, we list the compute infrastructure that we use to run all of the algorithms.

Table 5: Compute infrastructure.

CPU	GPU	Memory
AMD EPYC 7452	RTX3090×8	288GB

F Licences

We implement SAC on our own. Other codes are built upon source DDPG and TD3 codebases under MIT licence (<https://github.com/sfujim/TD3>), DARC codebase under MIT licence (<https://github.com/dmksjfl/DARC>), TQC codebase under MIT licence (https://github.com/SamsungLabs/tqc_pytorch), REDQ codebase under MIT licence (<https://github.com/watchernyu/REDQ>), DrQ-v2 codebase under MIT licence (<https://github.com/facebookresearch/drqv2>).

G Broader Impacts

This work mainly focuses on a simple and novel way of improving sample efficiency of the off-the-shelf off-policy RL algorithms. We do not foresee any potential negative social impact of this work.